

# Spectral measures and iterative bounds for effective diffusivity of steady and space-time periodic flows

N. B. Murphy, D. Hallman, E. Cherkaev, J. Xin, and K. M. Golden

## Abstract

Over three decades ago the advection-diffusion equation for a steady fluid velocity field was homogenized, leading to a Stieltjes integral representation for the effective diffusivity, which is given in terms of a spectral measure of a compact self-adjoint operator and the Péclet number of the fluid flow. This result was recently extended to space-time periodic flows, instead involving an unbounded self-adjoint operator. Padé approximants provide rigorous upper and lower bounds for Stieltjes functions in terms of the moments of the spectral measure. However, with the lack of a method for calculating the moments of the spectral measure for general fluid velocity fields, the utility of this powerful mathematical framework for calculating bounds for the effective diffusivity has not been fully realized. Here we significantly expand the applicability of this framework by providing an iterative method that enables an arbitrary number of moments, hence bounds, to be calculated analytically in closed form for both spatially and space-time periodic flows. The method is demonstrated for periodic flows in two spatial dimensions. The known asymptotic behavior of the effective diffusivity for a steady flow is accurately captured by high order upper and lower bounds, demonstrating the ability of the method to provide accurate estimates for the effective diffusivity for a broad range of parameter values.

## 1 Introduction

The long time large scale transport of passive tracers by an incompressible fluid velocity field is equivalent to a diffusion process [24] involving an effective diffusivity matrix  $\mathfrak{D}^*$  [12]. A Stieltjes integral representation for  $\mathfrak{D}^*$  was developed for steady flows, involving a spectral measure  $\mu$  of a compact self-adjoint operator [1, 2, 16]. Recently this result was extended to space-time periodic flows, involving a spectral measure for an unbounded self-adjoint operator [15]. This integral representation *separates* the Péclet number from the geometry and dynamics of the fluid velocity field, which is encoded in the spectral measure through its moments  $\mu^n$ . The theory of Padé approximants for Stieltjes functions provide a nested sequence of rigorous bounds for the diagonal components of the matrix  $\mathfrak{D}^*$ , given in terms of the measure moments [3]. The bounds get tighter as more moments are incorporated and can converge to the true value of  $\mathfrak{D}^*$  for certain Péclet number values [3]. However, for over 3 decades, the lack of a way to calculate the measure moments for general fluid velocity fields has hindered the progress of providing rigorous bounds for  $\mathfrak{D}^*$ .

Here, we develop an iterative method that, in principle, enables an arbitrary number of measure moments to be calculated analytically in *closed form* for any spatially periodic or space-time periodic fluid velocity field represented as a finite trigonometric Fourier series. This, in turn, enables an arbitrary number of nested bounds to be calculated for such flows. This iterative method is implemented into a numerical algorithm using Maple's symbolic math toolbox which can be used to calculate measure moments in closed form for such flows up to a given order only limited by computational resources. Moreover, we extend this numerical algorithm to Matlab, which enables hundreds of moments to be computed using floating point arithmetic. We incorporate the moment values into an existing numerical algorithm `padeapprox` [10] which computes Padé approximants in a robust, stable way and compute several nested bounds for the diagonal components of the matrix  $\mathfrak{D}^*$  for some model steady and space-time periodic flows. High order bounds accurately capture the known [6, 7] asymptotic behavior of the effective diffusivity for a steady cell-flow as a function of Péclet number in the advection dominated regime [15, 16]. Adding a space-time periodic term to the fluid velocity field of this steady flow results in an appreciable additional enhancement of  $\mathfrak{D}^*$ , shown both in the Padé

approximant bounds here and in numerical results involving direct computation of the spectral measure  $\mu$  [15].

The organization of the paper is as follows. In Section 2 the homogenization problem for the advection-diffusion equation is reviewed [12, 6, 17, 11]. In Section 2.1 an abstract Hilbert space framework is reviewed [15] which is used in Section 2.2 to provide Stieltjes integral representations for the components  $\mathfrak{D}_{jk}^*$ ,  $j, k = 1, \dots, d$ , of the effective diffusivity matrix  $\mathfrak{D}^*$  involving spectral measures  $\mu_{jk}$  of a self-adjoint operator [15], where  $d$  is the spatial dimension of the system. This abstract framework is utilized in Section 3 to develop an iterative method for calculating the moments  $\mu_{jk}^n$ ,  $n = 0, 1, 2, \dots$ , of  $\mu_{jk}$  for spatially and space-time periodic fluid velocity fields  $\mathbf{u}$ . The moments for a spatially and a space-time periodic  $\mathbf{u}$  are calculated in Section 4, which are incorporated into Padé approximant bounds for the diagonal components of  $\mathfrak{D}^*$  [3] in Section 5. Concluding remarks are given in Section 6.

## 2 Effective transport by advection-diffusion

The density  $\phi$  of a cloud of passive tracer particles diffusing along with molecular diffusivity  $\varepsilon$  and being advected by an incompressible velocity field  $\mathbf{u}$  satisfies the advection-diffusion equation

$$\partial_t \phi(t, \mathbf{x}) = \mathbf{u}(t, \mathbf{x}) \cdot \nabla \phi(t, \mathbf{x}) + \varepsilon \Delta \phi(t, \mathbf{x}), \quad \phi(0, \mathbf{x}) = \phi_0(\mathbf{x}), \quad (1)$$

for  $t > 0$  and  $\mathbf{x} \in \mathbb{R}^d$ . Here, the initial density  $\phi_0(\mathbf{x})$  and the fluid velocity field  $\mathbf{u}$  are assumed given, and  $\mathbf{u}$  satisfies  $\nabla \cdot \mathbf{u} = 0$ . In equation (1),  $\varepsilon > 0$  is the molecular diffusion constant,  $\partial_t$  denotes partial differentiation with respect to time  $t$ , and  $\Delta = \nabla \cdot \nabla = \nabla^2$  is the Laplacian. Moreover,  $\psi \cdot \varphi = \psi^T \overline{\varphi}$ , where  $\psi^T$  denotes transposition of the vector  $\psi$  and  $\overline{\varphi}$  denotes component-wise complex conjugation, with  $\psi \cdot \psi = |\psi|^2$ . Later, we will extensively use this form of the dot product over complex fields, with built in complex conjugation. However, we emphasize that all quantities considered in this section are *real-valued*.

In our analysis of the effective diffusivity matrix  $\mathfrak{D}^*$ , it is beneficial to use non-dimensional parameters. We therefore assume that equation (1) has been non-dimensionalized as follows. Let  $\ell$  and  $\tau$  be typical length and time scales associated with the problem of interest. Mapping to the non-dimensional variables  $t \mapsto t/\tau$  and  $\mathbf{x} \mapsto \mathbf{x}/\ell$ , one finds that  $\phi$  satisfies the advection diffusion equation in (1) with a non-dimensional molecular diffusivity and fluid velocity field,

$$\varepsilon \mapsto \tau \varepsilon / \ell^2, \quad \mathbf{u} \mapsto \tau \mathbf{u} / \ell. \quad (2)$$

This non-dimensionalization demonstrates that the fluid velocity field  $\mathbf{u}$  is divided by a quantity with dimensions of velocity and the molecular diffusivity is divided by a quantity with dimensions of velocity multiplied by spatial length. A detailed discussion of various non-dimensionalizations involving the Strouhal number, the Péclet number, and the periodic Péclet number is given in [13, 11]. It is convenient to choose the rescaled  $\mathbf{u}$  and  $\varepsilon$  in a way that captures information about the fluid velocity field. However, it is also convenient to choose these rescaled variables in a way that *separates* the rescaled  $\varepsilon$  from the *geometry and dynamics* of  $\mathbf{u}$ ; this leads to mathematically and physically meaningful properties of rigorous bounds for  $\mathfrak{D}^*$  which follow from the analytic structure of Stieltjes integral representations for  $\mathfrak{D}^*$  [2, 3] — discussed in Section 2.2 below.

We accomplish both of these goals as follows. Define the dimensional fluid velocity field by  $\mathbf{u} = u_0 \mathbf{v}$ , where the parameter  $u_0$  has dimensions of velocity and represents the “*flow strength*” of  $\mathbf{u}$  which is independent of the geometry and dynamics of  $\mathbf{u}$  which, in turn, is encapsulated in the non-dimensional vector field  $\mathbf{v}$ . With these definitions, we choose reference scales  $\tau$  and  $\ell$  in equation (2) to satisfy  $u_0 = \ell/\tau$  so that  $\mathbf{u} \mapsto \mathbf{v}$  and  $\varepsilon \mapsto \varepsilon/u_0 \ell$ . For example, for BC-flow [5], we define the dimensional fluid velocity field by  $\mathbf{u} = u_0 (C \cos y, B \cos x)$ , where the flow strength  $u_0 \in (0, \infty)$  is chosen to be independent of the non-dimensional parameters  $B, C \in [0, 1]$  which determine the streamline geometry of  $\mathbf{u}$  in  $\mathbf{v} = (C \cos y, B \cos x)$ .

An example of a non-dimensional parameter that compares the rate of scalar advection to the rate of diffusion is the Péclet number. We define it by the ratio  $Pe = \ell u_0 / \varepsilon$ , although other definitions have been used [13, 11, 11]. Therefore, our choice of the rescaled  $\varepsilon$  satisfies  $Pe = 1/\varepsilon$ . The advection and diffusion dominated regimes are characterized by  $Pe \gg 1$  and  $Pe \ll 1$ , respectively.

The *parameter separation* between  $Pe$  and the geometry of the flow is important for rigorous upper and lower Padé approximant bounds for  $\mathfrak{D}^*$  [2] discussed in Section 5. Padé approximants of  $\mathfrak{D}^*$  are given in

terms of ratios of polynomials [3]  $P(z)/Q(z)$ , where  $z = Pe^2$ ,  $0 < z < \infty$ , and the coefficients of these polynomials depend on the moments of a *spectral measure* that, in turn, depend on the fluid velocity field  $\mathbf{u}$  [2]. For example, when  $\mathbf{u}$  is given by *BC*-flow the moments of the measure depend on the parameters  $B$  and  $C$ . Our numerical investigations have shown if the non-dimensionalization of equation (1) is chosen in a way that the variable  $z$  also depends on the flow geometry through the ratio  $B/C$ , then this gives rise to *positive real* roots for the polynomials  $P(z)$  and  $Q(z)$ . This, in turn, gives rise to positive real roots and poles in the (rigorous) Padé approximant bounds for  $\mathfrak{D}^*$ , which is not physically or mathematically consistent with the known behavior of  $\mathfrak{D}^*$  [6, 18, 5, 11]. This demonstrates the importance of *parameter separation* between  $z$  and the flow geometry for Padé approximant bounds for  $\mathfrak{D}^*$ .

This way of non-dimensionalizing equation (1) is also convenient in the case of a time-dependent fluid velocity field [15], where the parameter  $u_0$  again represents the flow strength and the vector field  $\mathbf{v}$  encapsulates the *geometric and dynamical* properties of the flow. For example, the space-time periodic flow with velocity field  $\mathbf{u} = u_0((C \cos y, B \cos x) + \theta \cos t(\sin y, \sin x))$  has dynamical behavior exhibiting Lagrangian chaos [5, 15]. Here, the flow strength  $u_0 \in (0, \infty)$  is independent of the parameters  $B, C, \theta \in [0, 1]$  which determine the geometric and dynamical properties of  $\mathbf{u}$ . This choice of non-dimensionalization gives a clearer interpretation of the advection and diffusion dominated regimes in terms of  $Pe = 1/\varepsilon$  than the non-dimensionalization given in [15].

We now discuss the effective transport properties of advection enhanced diffusion, as described by the advection diffusion equation in (1). We will assume in this manuscript that the fluid velocity field  $\mathbf{u}$  is mean-zero in space for steady  $\mathbf{u} = \mathbf{u}(\mathbf{x})$  and mean-zero in space-time when  $\mathbf{u} = \mathbf{u}(t, \mathbf{x})$  is space-time dependent (also see [19]). The long time, large scale dispersion of diffusing tracers, such as heat or pollutants, being advected by an incompressible fluid velocity field is equivalent to an enhanced diffusion process [25] with an effective diffusivity matrix  $\mathfrak{D}^*$ . In recent decades, methods of homogenization theory [12, 6, 17, 11] have been used to provide an explicit representation for  $\mathfrak{D}^*$ . In particular, these methods have demonstrated that the averaged or *homogenized* behavior of the advection-diffusion equation in (1), with space-time periodic velocity field  $\mathbf{u}$ , is determined by a diffusion equation involving an averaged scalar density  $\bar{\phi}$  and an effective diffusivity tensor  $\mathfrak{D}^*$  [11]

$$\partial_t \bar{\phi}(t, \mathbf{x}) = \nabla \cdot [\mathfrak{D}^* \nabla \bar{\phi}(t, \mathbf{x})], \quad \bar{\phi}(0, \mathbf{x}) = \phi_0(\mathbf{x}). \quad (3)$$

Equation (3) follows from the assumption that the initial tracer density  $\phi_0$  varies slowly relative to the variations of the fluid velocity field  $\mathbf{u}$  [12, 7, 11]. This information is incorporated into equation (1) by introducing a small dimensionless parameter  $\delta \ll 1$  and writing [12, 7, 11]

$$\phi(0, \mathbf{x}) = \phi_0(\delta \mathbf{x}). \quad (4)$$

Anticipating that  $\phi$  will have diffusive dynamics as  $t \rightarrow \infty$ , space and time are rescaled according to the standard diffusive relation

$$\xi = \mathbf{x}/\delta, \quad \tau = t/\delta^2. \quad (5)$$

The rescaled form of equation (1) is given by [11]

$$\partial_t \phi^\delta(t, \mathbf{x}) = \delta^{-1} \mathbf{u}(t/\delta^2, \mathbf{x}/\delta) \cdot \nabla \phi^\delta(t, \mathbf{x}) + \varepsilon \Delta \phi^\delta(t, \mathbf{x}), \quad \phi^\delta(0, \mathbf{x}) = \phi_0(\mathbf{x}), \quad (6)$$

where we have denoted  $\phi^\delta(t, \mathbf{x}) = \phi(t/\delta^2, \mathbf{x}/\delta)$ . The convergence of  $\phi^\delta$  to  $\bar{\phi}$  can be rigorously established in the following sense [11]

$$\lim_{\delta \rightarrow 0} \sup_{0 \leq t \leq t_0} \sup_{\mathbf{x} \in \mathbb{R}^d} |\phi^\delta(t, \mathbf{x}) - \bar{\phi}(t, \mathbf{x})| = 0, \quad (7)$$

for every finite  $t_0 > 0$ , provided that  $\phi_0$  and  $\mathbf{u}$  obey some mild smoothness and boundedness conditions.

An explicit representation of the effective diffusivity tensor  $\mathfrak{D}^*$  is given in terms of the (unique) mean zero, space-time periodic solution  $\chi_j$  of the following *cell problem* [5, 11],

$$\partial_\tau \chi_j(\tau, \xi) - \varepsilon \Delta_\xi \chi_j(\tau, \xi) - \mathbf{u}(\tau, \xi) \cdot \nabla_\xi \chi_j(\tau, \xi) = u_j(\tau, \xi), \quad (8)$$

where the subscript  $\xi$  in  $\Delta_\xi$  and  $\nabla_\xi$  indicates that differentiation is with respect to the fast variable  $\xi$  defined in equation (5). The components  $\mathfrak{D}_{jk}^*$ ,  $j, k = 1, \dots, d$ , of the matrix  $\mathfrak{D}^*$  are given by [12, 6, 17, 11]

$$\mathfrak{D}_{jk}^* = \varepsilon \delta_{jk} + \langle u_j \chi_k \rangle, \quad (9)$$

where  $\delta_{jk}$  is the Kronecker delta and  $u_j$  is the  $j$ th component of the vector  $\mathbf{u}$ . The averaging  $\langle \cdot \rangle$  in (9) is with respect to the fast variables defined in equation (5). The averaging is over the bounded sets  $\mathcal{T} \subset \mathbb{R}$  and  $\mathcal{V} \subset \mathbb{R}^d$ , with  $\tau \in \mathcal{T}$  and  $\xi \in \mathcal{V}$ , which define the space-time period cell  $((d+1)\text{-torus}) \mathcal{T} \times \mathcal{V}$ .

In general, the effective diffusivity tensor  $\mathfrak{D}^*$  has a symmetric  $\mathfrak{S}^*$  and antisymmetric  $\mathfrak{A}^*$  part defined by

$$\mathfrak{D}^* = \mathfrak{S}^* + \mathfrak{A}^*, \quad \mathfrak{S}^* = \frac{1}{2} (\mathfrak{D}^* + [\mathfrak{D}^*]^T), \quad \mathfrak{A}^* = \frac{1}{2} (\mathfrak{D}^* - [\mathfrak{D}^*]^T), \quad (10)$$

where  $[\mathfrak{D}^*]^T$  denotes transposition of the matrix  $\mathfrak{D}^*$ . Denote by  $\mathfrak{S}_{jk}^*$  and  $\mathfrak{A}_{jk}^*$ ,  $j, k = 1, \dots, d$ , the components of  $\mathfrak{S}^*$  and  $\mathfrak{A}^*$  in (10). When the fluid velocity field is mean-zero and divergence-free, as discussed above, then equation (7) holds and the effective diffusivity tensor  $\mathfrak{D}^*$  defined in (9) is constant [11]. Consequently, only the symmetric part of  $\mathfrak{D}^*$  plays a role in the effective transport equation shown in (3), as the antisymmetric part of  $\mathfrak{D}^*$  cancels out in the sum  $\sum_{ij} \mathfrak{D}_{ij}^* \partial_i \partial_j \bar{\phi}$ , where  $\partial_i$  denotes differentiation in the  $i$ th spatial direction [18].

In Section 4.3 we consider the fluid velocity field  $\mathbf{u}$

$$\mathbf{u}(t, \mathbf{x}) = (C \cos y, B \cos x) + \theta \cos t (\sin y, \sin x), \quad \theta \in [0, 1]. \quad (11)$$

with temporal periodicity  $\mathcal{T} = [0, 2\pi]$  and spatial periodicity  $\mathcal{V} = [0, 2\pi]^d$ , with  $d = 2$ . In the case of a time-dependent fluid velocity field,  $\langle \cdot \rangle$  denotes space-time averaging over  $\mathcal{T} \times \mathcal{V}$ . In the special case of a time-independent fluid velocity field, the function  $\chi_j$  is time-independent and satisfies equation (8) with  $\partial_\tau \chi_j \equiv 0$ , and  $\langle \cdot \rangle$  in (9) denotes spatial averaging over  $\mathcal{V}$  [6, 17, 11].

## 2.1 Hilbert space

In this section we provide an abstract Hilbert space formulation of the effective parameter problem for advection-diffusion that was proposed in [18], based on [4], and generalized to the setting of a space-time periodic fluid velocity field in [15]. To fix ideas, consider the following sets  $\mathcal{T} = [0, T]$  and  $\mathcal{V} = \otimes_{j=1}^d [0, L]$  which define the space-time period cell  $\mathcal{T} \times \mathcal{V}$ . Now consider the Hilbert spaces  $L^2(\mathcal{T})$  and  $L^2(\mathcal{V})$  of Lebesgue measurable scalar functions over the complex field  $\mathbb{C}$  that are also square integrable [9]. Define the associated Hilbert spaces  $\mathcal{H}_\mathcal{T}$ ,  $\mathcal{H}_\mathcal{V}$ , and  $\mathcal{H}_{\mathcal{T}\mathcal{V}} = \mathcal{H}_\mathcal{T} \otimes \mathcal{H}_\mathcal{V}$  of periodic functions, where

$$\begin{aligned} \mathcal{H}_\mathcal{T} &= \{ \psi \in L^2(\mathcal{T}) \mid \psi(t) = \psi(t+T) \}, \\ \mathcal{H}_\mathcal{V} &= \{ \psi \in L^2(\mathcal{V}) \mid \psi(\mathbf{x}) = \psi(\mathbf{x} + L\mathbf{e}_j), \ j = 1, \dots, d \}, \end{aligned} \quad (12)$$

and the  $\mathbf{e}_j$  are standard basis vectors.

More specifically, denote time average over  $\mathcal{T}$  by  $\langle \cdot \rangle_\mathcal{T}$ , space average over  $\mathcal{V}$  by  $\langle \cdot \rangle_\mathcal{V}$ , and space-time average over  $\mathcal{T} \times \mathcal{V}$  by  $\langle \cdot \rangle$ . The space-time average  $\langle \cdot \rangle$ , induces a sesquilinear inner-product  $\langle \cdot, \cdot \rangle$  given by  $\langle \psi, \varphi \rangle = \langle \psi | \varphi \rangle$ , with  $\langle \varphi, \psi \rangle = \overline{\langle \psi, \varphi \rangle}$ . This  $\mathcal{H}_{\mathcal{T}\mathcal{V}}$ -inner-product, in turn, induces a norm  $\| \cdot \|$  given by  $\| \psi \| = \langle \psi, \psi \rangle^{1/2}$  [9]. The set of space-time periodic Lebesgue measurable functions  $\mathcal{H}_{\mathcal{T}\mathcal{V}}$  satisfying  $\| f \| < \infty$  is a (complete) Hilbert space [9]. Similarly, the space and time averages,  $\langle \cdot \rangle_\mathcal{V}$  and  $\langle \cdot \rangle_\mathcal{T}$ , induce sesquilinear inner-products,  $\langle \cdot, \cdot \rangle_\mathcal{V}$  and  $\langle \cdot, \cdot \rangle_\mathcal{T}$ , that induce norms,  $\| \cdot \|_\mathcal{V}$  and  $\| \cdot \|_\mathcal{T}$ , associated with the Hilbert spaces  $\mathcal{H}_\mathcal{V}$  and  $\mathcal{H}_\mathcal{T}$ .

To treat temporal dependence, we define the space  $\mathcal{A}_\mathcal{T}$  of functions that are absolutely continuous [23, 21] on the interval  $\mathcal{T}$ , having derivative belonging to  $L^2(\mathcal{T})$ , and the space  $\tilde{\mathcal{A}}_\mathcal{T}$  of absolutely continuous  $\mathcal{T}$ -periodic functions with time derivatives belonging to  $L^2(\mathcal{T})$ ,

$$\tilde{\mathcal{A}}_\mathcal{T} = \{ \psi \in \mathcal{A}_\mathcal{T} \mid \psi(0) = \psi(T) \}, \quad (13)$$

which is *not* a Hilbert space but is instead an everywhere dense subset of the Hilbert space  $\mathcal{H}_\mathcal{T}$  [23]. To treat spatial dependence, we now define the Sobolev space  $\mathcal{H}_\mathcal{V}^{1,2}$  which is itself a Hilbert space [4, 8, 14],

$$\mathcal{H}_\mathcal{V}^{1,2} = \{ \psi \in \mathcal{H}_\mathcal{V} \mid \|\nabla \psi\|_\mathcal{V} < \infty, \langle \psi \rangle_\mathcal{V} = 0 \}. \quad (14)$$

The condition  $\langle \psi \rangle_{\mathcal{V}} = 0$  in (14) is required to eliminate non-zero constant  $\psi$ , which satisfies  $\|\nabla \psi\|_{\mathcal{V}} = 0$ . The  $\mathcal{H}_{\mathcal{V}}^{1,2}$ -norm  $\|\nabla \cdot\|_{\mathcal{V}}$  is induced by the  $\mathcal{H}_{\mathcal{V}}^{1,2}$ -inner-product:  $\|\nabla \psi\|_{\mathcal{V}} = \langle \nabla \psi \cdot \nabla \psi \rangle_{\mathcal{V}}^{1/2}$ .

Finally, define the Hilbert space  $\mathcal{H}$  and its everywhere dense subset  $\mathcal{F}$

$$\mathcal{H} = \mathcal{H}_{\mathcal{T}} \otimes \mathcal{H}_{\mathcal{V}}^{1,2}, \quad \mathcal{F} = \tilde{\mathcal{A}}_{\mathcal{T}} \otimes \mathcal{H}_{\mathcal{V}}^{1,2}. \quad (15)$$

Due to the presence of  $\tilde{\mathcal{A}}_{\mathcal{T}}$  in the definition of the function space  $\mathcal{F}$ , it is *not* a complete Hilbert space, and is instead an everywhere dense subset of the complete Hilbert space  $\mathcal{H}$ . Recall that  $\langle \cdot \rangle$  denotes space-time average over  $\mathcal{T} \times \mathcal{V}$  and  $\psi \cdot \zeta = \psi^T \zeta$ . The sesquilinear  $\mathcal{H}$ -inner-product is given by  $\langle \psi, \varphi \rangle_{1,2} = \langle \nabla \psi \cdot \nabla \varphi \rangle$  with associated norm  $\|\cdot\|_{1,2}$  given by  $\|\psi\|_{1,2} = \langle |\nabla \psi|^2 \rangle^{1/2}$ . We emphasize that in the case of a time-dependent fluid velocity field, it is necessary that  $\psi \in \mathcal{H}$  satisfy  $\langle \psi \rangle_{\mathcal{V}} = 0$ , as required by the definition of  $\mathcal{H}_{\mathcal{V}}^{1,2}$  in (14). Otherwise,  $\|\cdot\|_{1,2} = |\mathcal{T} \times \mathcal{V}|^{-1} \int_{\mathcal{T} \times \mathcal{V}} dt dx |\nabla \cdot|^2$  is not a norm, since a strictly positive function  $\psi(t, \mathbf{x}) = \psi(t)$  on  $\mathcal{T} \times \mathcal{V}$  satisfies  $\|\psi\|_{1,2} = 0$ , where  $|\mathcal{T} \times \mathcal{V}|$  denotes Lebesgue measure of the set  $\mathcal{T} \times \mathcal{V}$ . In the case of a time-independent fluid velocity field  $\mathbf{u} = \mathbf{u}(\mathbf{x})$  we set  $\mathcal{H} \equiv \mathcal{F} \equiv \mathcal{H}_{\mathcal{V}}^{1,2}$ , and  $\langle \cdot \rangle = \langle \cdot \rangle_{\mathcal{V}}$ .

## 2.2 Integral representations for the effective diffusivity

In this section we summarize the results of [15], which provides Stieltjes integral representations for both the symmetric  $\mathfrak{S}^*$  and antisymmetric  $\mathfrak{A}^*$  parts of  $\mathfrak{D}^*$ . Since the analysis in this section involves only the fast variables  $(\tau, \xi)$  defined in equation (5), for notational simplicity, we will drop the subscripts  $\xi$  shown in equation (8) and use  $\partial_t$  to denote  $\partial_{\tau}$ .

Inserting the expression for  $u_j$  on the right side of (8) into equation (9) leads to the following functional representations for the components  $\mathfrak{S}_{jk}^*$  and  $\mathfrak{A}_{jk}^*$ ,  $j, k = 1, \dots, d$ , of  $\mathfrak{S}^*$  and  $\mathfrak{A}^*$  [18]

$$\mathfrak{S}_{jk}^* = \varepsilon(\delta_{jk} + \langle \chi_j, \chi_k \rangle_{1,2}), \quad \mathfrak{A}_{jk}^* = \langle A\chi_j, \chi_k \rangle_{1,2}, \quad A = (-\Delta)^{-1}(\partial_t - \mathbf{u} \cdot \nabla). \quad (16)$$

Here,  $\langle f, h \rangle_{1,2} = \langle \nabla f \cdot \nabla h \rangle$  is a Sobolev-type *sesquilinear* inner-product [14] and the operator  $(-\Delta)^{-1}$  is based on convolution with respect to the Green's function for the Laplacian  $\Delta$  [22, 8]. Since the function  $\chi_j$  is *real-valued* we have  $\langle \chi_j, \chi_k \rangle_{1,2} = \langle \chi_k, \chi_j \rangle_{1,2}$ , which implies that  $\mathfrak{S}^*$  is a symmetric matrix. The function  $A\chi_j$  is also real-valued. The operator  $A$  is skew-adjoint on the Hilbert space  $\mathcal{H}$  [15], which implies that  $\mathfrak{A}_{kj}^* = \langle A\chi_k, \chi_j \rangle_{1,2} = -\langle \chi_k, A\chi_j \rangle_{1,2} = -\langle A\chi_j, \chi_k \rangle_{1,2} = -\mathfrak{A}_{jk}^*$  which, in turn, implies that  $\mathfrak{A}^*$  is an antisymmetric matrix, hence  $\mathfrak{A}_{kk}^* = \langle A\chi_k, \chi_k \rangle_{1,2} = 0$ .

Applying the linear operator  $(-\Delta)^{-1}$  to both sides of the cell problem in equation (8) yields the following resolvent formula for  $\chi_j$

$$\chi_j = (\varepsilon + A)^{-1}g_j, \quad g_j = (-\Delta)^{-1}u_j. \quad (17)$$

From equations (16) and (17) we have the following functional formulas for  $\mathfrak{S}_{jk}^*$  and  $\mathfrak{A}_{jk}^*$  involving the skew-adjoint operator  $A$

$$\begin{aligned} \mathfrak{S}_{jk}^* &= \varepsilon(\delta_{jk} + \langle (\varepsilon + A)^{-1}g_j, (\varepsilon + A)^{-1}g_k \rangle_{1,2}), \\ \mathfrak{A}_{jk}^* &= \langle A(\varepsilon + A)^{-1}g_j, (\varepsilon + A)^{-1}g_k \rangle_{1,2}. \end{aligned} \quad (18)$$

Since  $A$  is a skew-adjoint operator, it can be written as  $A = iM$  where  $M$  is a symmetric operator [23]. In [15] it is shown that  $M$  is *self-adjoint* on the Hilbert space  $\mathcal{H}$ .

The spectral theorem for self-adjoint operators states that there is a one-to-one correspondence between the self-adjoint operator  $M$  and a family of self-adjoint projection operators  $\{Q(\lambda)\}_{\lambda \in \Sigma}$  — the resolution of the identity — that satisfies  $\lim_{\lambda \rightarrow \inf \Sigma} Q(\lambda) = 0$  and  $\lim_{\lambda \rightarrow \sup \Sigma} Q(\lambda) = I$  [23]. Here,  $\Sigma$  is the *spectrum* of the operator  $M$ , while  $0$  and  $I$  denote the null and identity operators. Define the *complex valued* function  $\mu_{jk}(\lambda) = \langle Q(\lambda)g_j, g_k \rangle_{1,2}$ ,  $j, k = 1, \dots, d$ , where  $g_j = (-\Delta)^{-1}u_j$  is defined in (17). The real,  $\text{Re } \mu_{jk}(\lambda)$ , and imaginary,  $\text{Im } \mu_{jk}(\lambda)$ , parts of the function  $\mu_{jk}(\lambda)$  are of bounded variation, and therefore have Stieltjes measures  $\text{Re } \mu_{jk}$  and  $\text{Im } \mu_{jk}$  associated with them [23]. The function  $\mu_{kk}(\lambda)$  is positive hence  $\mu_{kk}$  is a positive measure, while  $\text{Re } \mu_{jk}$  and  $\text{Im } \mu_{jk}$ ,  $j \neq k$ , are signed measures. Given certain regularity conditions [15] on the components  $u_j$  of the fluid velocity field  $\mathbf{u}$ , the functional formulas for  $\mathfrak{S}_{jk}^*$  and  $\mathfrak{A}_{jk}^*$  in (18) have the

following Radon–Stieltjes integral representations, for all  $0 < \varepsilon < \infty$

$$\mathfrak{S}_{jk}^* = \varepsilon \left( \delta_{jk} + \int_{-\infty}^{\infty} \frac{d\text{Re } \mu_{jk}(\lambda)}{\varepsilon^2 + \lambda^2} \right), \quad \mathfrak{A}_{jk}^* = - \int_{-\infty}^{\infty} \frac{\lambda d\text{Im } \mu_{jk}(\lambda)}{\varepsilon^2 + \lambda^2}. \quad (19)$$

The integration in (19) is over the spectrum  $\Sigma \subseteq \mathbb{R}$  of the self-adjoint operator  $M = -\imath A$  [23, 20]. In the setting of a time-independent flow,  $\mathbf{u} = \mathbf{u}(\mathbf{x})$ , the operator  $A = (-\Delta)^{-1}[\mathbf{u} \cdot \nabla]$  and the self-adjoint operator  $M = -\imath A$  is compact [4]. Therefore, the spectrum  $\Sigma$  is discrete outside a neighborhood of  $\lambda = 0$  with a limit point at  $\lambda = 0$  [22]. In the setting of a time-dependent flow,  $\mathbf{u} = \mathbf{u}(t, \mathbf{x})$ ,  $M = -\imath A$  is an unbounded operator [15, 23]. Therefore, in general, the spectrum  $\Sigma$  can be an unbounded subset of  $\mathbb{R}$ , it can have discrete and continuous components, and can even coincide with  $\mathbb{R}$  itself [23].

### 3 Iterative moment method

In this section we provide an iterative method which may be used to calculate, in principle, an arbitrary number of moments for spectral measures associated with the effective diffusivity for spatially and space-time periodic fluid velocity fields. The spectral theorem shows that the mass  $\mu_{jk}^0$  and the moments  $\mu_{jk}^n$ ,  $n = 1, 2, 3, \dots$ , of the spectral measure  $\mu_{jk}$  are given by

$$\mu_{jk}^0 = \int_{-\infty}^{\infty} d\mu_{jk}(\lambda) = \langle g_j, g_k \rangle_{1,2}, \quad \mu_{jk}^n = \int_{-\infty}^{\infty} \lambda^n d\mu_{jk}(\lambda) = \langle M^n g_j, g_k \rangle_{1,2}, \quad n = 1, 2, 3, \dots,$$

where  $M = -\imath A$  and the operator  $M^n$  is defined through composition. Integration by parts and properties of the operator  $(-\Delta)^{-1}$  show that the mass  $\mu_{jk}^0$  of the measure  $\mu_{jk}$  is given by [15]

$$\mu_{jk}^0 = \langle g_j, g_k \rangle_{1,2} = \langle \nabla(-\Delta)^{-1} u_j \cdot \nabla(-\Delta)^{-1} u_k \rangle = \langle (-\Delta)^{-1} u_j, u_k \rangle_2 = \langle g_j, u_k \rangle_2, \quad (20)$$

where we have denoted  $\langle \cdot, \cdot \rangle_2$  the sesquilinear  $L^2(\mathcal{T} \times \mathcal{V})$  inner-product. Similarly, denoting the *material derivative*  $D_t = \partial_t + \mathbf{u} \cdot \nabla$  for time-dependent  $\mathbf{u}$  and  $D_t = \mathbf{u} \cdot \nabla$  for time-independent  $\mathbf{u}$ , with  $A = (-\Delta)^{-1} D_t$ , integration by parts and the anti-symmetry of  $A$  yield [15]

$$\begin{aligned} \mu_{jk}^1 &= \langle M g_j, g_k \rangle_{1,2} = -\imath \langle D_t g_j, g_k \rangle_2, \\ \mu_{jk}^2 &= \langle M^2 g_j, g_k \rangle_{1,2} = \langle A g_j, A g_k \rangle_{1,2} = \langle D_t g_j, A g_k \rangle_2. \end{aligned} \quad (21)$$

Higher moments are found in a similar way, for  $n = 1, 2, 3, \dots$ ,

$$\begin{aligned} \mu_{jk}^{2n+1} &= \langle M^{2n+1} g_j, g_k \rangle_{1,2} = -\imath \langle A^{n+1} g_j, A^n g_k \rangle_{1,2} = -\imath \langle D_t A^n g_j, A^n g_k \rangle_2, \\ \mu_{jk}^{2n+2} &= \langle M^{2n+2} g_j, g_k \rangle_{1,2} = \langle A^{n+1} g_j, A^{n+1} g_k \rangle_{1,2} = \langle D_t A^n g_j, A^{n+1} g_k \rangle_2. \end{aligned} \quad (22)$$

From equation (22) and the asymmetry of  $A$ , we have  $\mu_{jk}^{2n+1} = 0$  for all  $n = 0, 1, 2, \dots$  [15]. Moreover,  $\mu_{jk}^{2n} = \mu_{jk}^{2n}$  as  $g_k$ ,  $D_t g_k$ ,  $A^n g_k$ , and  $D_t A^n g_k$  are real-valued functions for all  $n = 1, 2, \dots$ . In summary,

$$\mu_{kj}^{2n} = \mu_{jk}^{2n}, \quad \mu_{jk}^{2n+1} = 0. \quad (23)$$

A key property of the operators  $(-\Delta)^{-1}$ ,  $D_t$ , and  $A = (-\Delta)^{-1} D_t$  is that they are *linear*. In order to take advantage of this property in our calculation of the moments  $\mu_{jk}^n$  of the measure  $\mu_{jk}$ , we take  $\mathcal{T} = [0, 2\pi]$  and  $\mathcal{V} = [0, 2\pi]^2$ , and write the fluid velocity field  $\mathbf{u}$  in the complex, orthonormal Fourier basis for  $L^2(\mathcal{T} \times \mathcal{V})$  [9]

$$\mathbf{u} = \sum_{\ell, \mathbf{k}} \mathbf{a}_{\ell, \mathbf{k}} \phi_{\ell, \mathbf{k}}, \quad \phi_{\ell, \mathbf{k}}(t, \mathbf{x}) = \exp[\imath(\ell t + \mathbf{k} \cdot \mathbf{x})], \quad \mathbf{a}_{\ell, \mathbf{k}} = \langle \mathbf{u}, \phi_{\ell, \mathbf{k}} \rangle_2, \quad (24)$$

where  $\ell \in \mathbb{Z}$ ,  $\mathbf{k} \in \mathbb{Z}^d$ ,  $\mathbf{a}_{\ell, \mathbf{k}} = (a_{\ell, \mathbf{k}}^1, \dots, a_{\ell, \mathbf{k}}^d)$ , and the average  $\langle \mathbf{u}, \phi_{\ell, \mathbf{k}} \rangle_2$  is understood to be component-wise, so  $(\mathbf{a}_{\ell, \mathbf{k}})_i = \langle u_i, \phi_{\ell, \mathbf{k}} \rangle_2$ . The orthonormal basis vectors satisfy

$$\langle \phi_{\ell, \mathbf{k}}, \phi_{\ell', \mathbf{k}'} \rangle_2 = \langle \phi_{\ell - \ell', \mathbf{k} - \mathbf{k}'} \rangle = \delta_{\ell, \ell'} \delta_{\mathbf{k}, \mathbf{k}'}, \quad (25)$$

where  $\langle \cdot \rangle$  denotes averaging over  $\mathcal{T} \times \mathcal{V}$  and  $\delta_{i,j}$  is the Kronecker delta, with  $\delta_{\mathbf{k},\mathbf{k}'} = \prod_i \delta_{k_i, k'_i}$ . For simplicity, we assume that there are a *finite* number of terms in the Fourier expansion of  $\mathbf{u}$ . In the setting of a time-independent flow,  $\mathbf{u} = \mathbf{u}(\mathbf{x})$ , the basis function  $\phi_{\ell,\mathbf{k}}$  is replaced by  $\phi_{\mathbf{k}}(\mathbf{x}) = \exp(i \mathbf{k} \cdot \mathbf{x})$ , so that  $\mathbf{a}_{\ell,\mathbf{k}} = \mathbf{a}_{0,\mathbf{k}} = \mathbf{a}_{\mathbf{k}}$ . The basis functions  $\{\phi_{\ell,\mathbf{k}}\}_{\ell,\mathbf{k}}$  are *eigenfunctions* of the operators  $\partial_t$ ,  $\nabla$ , and  $(-\Delta)^{-1}$ , with [15]

$$\partial_t \phi_{\ell,\mathbf{k}} = i\ell \phi_{\ell,\mathbf{k}}, \quad \nabla \phi_{\ell,\mathbf{k}} = i\mathbf{k} \phi_{\ell,\mathbf{k}}, \quad (-\Delta)^{-1} \phi_{\ell,\mathbf{k}} = |\mathbf{k}|^{-2} \phi_{\ell,\mathbf{k}}. \quad (26)$$

It follows from equations (24) and (26), and the linearity of the operator  $(-\Delta)^{-1}$  that  $g_j = (-\Delta)^{-1} u_j$  satisfies

$$g_j = \sum_{\ell,\mathbf{k}} |\mathbf{k}|^{-2} a_{\ell,\mathbf{k}}^j \phi_{\ell,\mathbf{k}}. \quad (27)$$

Moreover, from equation (26),  $D_t = \partial_t + \mathbf{u} \cdot \nabla$ , and  $A = (-\Delta)^{-1} D_t$ , we have

$$\begin{aligned} D_t \phi_{\ell',\mathbf{k}'} &= (\partial_t + \mathbf{u} \cdot \nabla) \phi_{\ell',\mathbf{k}'} \\ &= i\ell' \phi_{\ell',\mathbf{k}'} + [\mathbf{u} \cdot i\mathbf{k}'] \phi_{\ell',\mathbf{k}'} \\ &= i\ell' \phi_{\ell',\mathbf{k}'} - \sum_{\ell,\mathbf{k}} i[\mathbf{a}_{\ell,\mathbf{k}} \cdot \mathbf{k}'] \phi_{\ell'+\ell,\mathbf{k}'+\mathbf{k}} \\ A \phi_{\ell',\mathbf{k}'} &= i\ell' |\mathbf{k}'|^{-2} \phi_{\ell',\mathbf{k}'} - \sum_{\ell,\mathbf{k}} i[\mathbf{a}_{\ell,\mathbf{k}} \cdot \mathbf{k}'] |\mathbf{k}' + \mathbf{k}|^{-2} \phi_{\ell'+\ell,\mathbf{k}'+\mathbf{k}}, \end{aligned} \quad (28)$$

where the  $-i$  comes from the sesquilinearity of the dot product. Consequently, equations (27) and (28), and the linearity of the operators  $D_t$  and  $A$  yield

$$D_t g_j = \sum_{\ell,\mathbf{k}} |\mathbf{k}|^{-2} a_{\ell,\mathbf{k}}^j D_t \phi_{\ell,\mathbf{k}}, \quad A g_j = \sum_{\ell,\mathbf{k}} |\mathbf{k}|^{-2} a_{\ell,\mathbf{k}}^j A \phi_{\ell,\mathbf{k}}. \quad (29)$$

The mass and moments of the spectral measure  $\mu_{jk}$  can be expressed explicitly in terms of just the Fourier coefficients  $\mathbf{a}_{\ell,\mathbf{k}}$  of  $\mathbf{u}$ , using the orthonormality of the basis  $\{\phi_{\ell,\mathbf{k}}\}$  and equations (20)–(24), (27) and (29). For example equations (20), (24), and (27), and the orthonormality of the  $\phi_{\ell,\mathbf{k}}$  yield

$$\mu_{jk}^0 = \langle (-\Delta)^{-1} u_j, u_k \rangle_2 = \sum_{\ell,\mathbf{k}} |\mathbf{k}|^{-2} a_{\ell,\mathbf{k}}^j \bar{a}_{\ell,\mathbf{k}}^k, \quad (30)$$

where  $\bar{a}_{\ell,\mathbf{k}}^j$  is the complex conjugate of  $a_{\ell,\mathbf{k}}^j$ . Similarly, the first  $\mu_{jk}^1$  and second  $\mu_{jk}^2$  moments of the measure  $\mu_{jk}$  can be expressed explicitly in terms of just the Fourier coefficients  $\mathbf{a}_{\ell,\mathbf{k}}$  of  $\mathbf{u}$ . However, these equations expressed in terms of the  $\mathbf{a}_{\ell,\mathbf{k}}$  are complicated and those for higher moments  $\mu_{jk}^n$ ,  $n = 3, 4, \dots$ , expressed in terms of the  $\mathbf{a}_{\ell,\mathbf{k}}$  become unmanageable. However, the form of the formulas for  $\mu_{jk}^n$  in equations (21) and (22) show that an arbitrary number of the moments can be found *iteratively*.

The key to doing so is determining how the operators  $(-\Delta)^{-1}$ ,  $D_t = \mathbf{u} \cdot \nabla$ , and  $A = (-\Delta)^{-1} D_t$  map one iterate to the next. By linearity, it suffices to understand how these operators transform a single Fourier mode  $p_{\ell,\mathbf{k}} \phi_{\ell,\mathbf{k}}$  to potentially multiple modes  $\sum_{\ell',\mathbf{k}'} p'_{\ell',\mathbf{k}'} \phi_{\ell',\mathbf{k}'}$ . By equations (24), (26) and (28), we have

$$\begin{aligned} (-\Delta)^{-1} \phi_{\ell',\mathbf{k}'} &= |\mathbf{k}'|^{-2} \phi_{\ell',\mathbf{k}'}, \\ D_t \phi_{\ell',\mathbf{k}'} &= i\ell' \phi_{\ell',\mathbf{k}'} - \sum_{\ell,\mathbf{k}} i[\mathbf{a}_{\ell,\mathbf{k}} \cdot \mathbf{k}'] \phi_{\ell'+\ell,\mathbf{k}'+\mathbf{k}}, \\ A \phi_{\ell',\mathbf{k}'} &= i\ell' |\mathbf{k}'|^{-2} \phi_{\ell',\mathbf{k}'} - \sum_{\ell,\mathbf{k}} i[\mathbf{a}_{\ell,\mathbf{k}} \cdot \mathbf{k}'] |\mathbf{k}' + \mathbf{k}|^{-2} \phi_{\ell'+\ell,\mathbf{k}'+\mathbf{k}}, \end{aligned} \quad (31)$$

To make this explicit, we write

$$u_j = \sum_{\ell,\mathbf{k}} a_{\ell,\mathbf{k}}^j \phi_{\ell,\mathbf{k}}, \quad g_j = \sum_{\ell,\mathbf{k}} b_{\ell,\mathbf{k}}^j \phi_{\ell,\mathbf{k}}, \quad D_t g_j = \sum_{\ell,\mathbf{k}} c_{\ell,\mathbf{k}}^j \phi_{\ell,\mathbf{k}}, \quad A g_j = \sum_{\ell,\mathbf{k}} d_{\ell,\mathbf{k}}^j \phi_{\ell,\mathbf{k}}. \quad (32)$$

Therefore, equations (20), (21), and (32), and the orthonormality of the  $\phi_{\ell,k}$  yield

$$\mu_{jk}^0 = \sum_{\ell,k} b_{\ell,k}^j \bar{a}_{\ell,k}^k, \quad \mu_{jk}^1 = -i \sum_{\ell,k} c_{\ell,k}^j \bar{b}_{\ell,k}^k, \quad \mu_{jk}^2 = \sum_{\ell,k} c_{\ell,k}^j \bar{d}_{\ell,k}^k. \quad (33)$$

In a similar way, for each  $n = 1, 2, 3, \dots$ , denote

$$D_t A^n g_j = \sum_{\ell,k} c_{\ell,k}^{j,n} \phi_{\ell,k}, \quad A^n g_j = \sum_{\ell,k} d_{\ell,k}^{j,n} \phi_{\ell,k}, \quad (34)$$

with  $d_{\ell,k}^{j+1} = d_{\ell,k}^j$  and  $d_{\ell,k}^{j,n} = |\mathbf{k}|^{-2} c_{\ell,k}^{j,n}$ . Then, from equation (22) we have

$$\mu_{jk}^{2n+1} = -i \sum_{\ell,k} c_{\ell,k}^{j,n} \bar{d}_{\ell,k}^{k,n}, \quad \mu_{jk}^{2n+2} = \sum_{\ell,k} c_{\ell,k}^{j,n} \bar{d}_{\ell,k}^{k,n+1}. \quad (35)$$

In the next section we will use the iterative mappings in (31) and formulas for the spectral measure mass and moments in equations (33) and (35) to calculate many moments for some steady and space-time periodic fluid flows.

## 4 Moment calculations

In this section we analytically and numerically calculate moments  $\mu_{jk}^{2n}$ , for  $n = 0, 1, 2, \dots$ , and  $j, k = 1, \dots, d$ , for each of the spectral measures  $\mu_{jk}$ . For shear flow we analytically calculate all of the moments. These results show that each of the spectral measures is a  $\delta$ -function centered at the spectral origin. For 2D steady BC-flow and a related time-dependent 2D flow, we implement the iterative moment method developed in Section 3 using Maple's symbolic math toolbox and calculate several moments analytically in closed form. We also implement the iterative moment method in Matlab and compute many more moments to floating point precision. In Section 5, we incorporate the positive moment values  $\mu_{kk}^{2n}$  in Padé approximant bounds for the diagonal components  $\mathfrak{D}_{kk}^*$  of the effective diffusivity matrix  $\mathfrak{D}^*$  for these 2D fluid velocity fields.

### 4.1 Moments of shear flow

We now consider the special case of shear flow. The fluid velocity field for shear flow is time-independent. In 2D shear flow in the  $x$ -direction has a fluid velocity  $\mathbf{u} = (0, \zeta(x))$  and  $\mathbf{u} = (\xi(y), 0)$  for flow in the  $y$ -direction, where in the current context  $\xi$  and  $\zeta$  are arbitrary mean-zero functions which are expressible by finite Fourier series, as shown in equation in (24). Examples of 3D shear flow fluid velocity fields are  $\mathbf{u} = (\xi(y, z), 0, 0)$ ,  $\mathbf{u} = (0, \zeta(x, z), 0)$ , and  $\mathbf{u} = (0, 0, \gamma(x, y))$ , where  $\gamma$  is also an arbitrary function of the same type as  $\xi$  and  $\zeta$ .

The key property of these simple shear flows is that only one component of the fluid velocity field is non-zero, the  $i$ th component say, and that component is a function which is independent of  $x_i$ , the  $i$ th component of  $\mathbf{x}$ . This property and equations (26) and (27) imply  $\nabla g_j = 0$  for all  $j = 1, \dots, d$ , hence  $D_t g_j = \mathbf{u} \cdot \nabla g_j = 0$  for all  $j = 1, \dots, d$  which, in turn, implies that  $A g_j = (-\Delta)^{-1} D_t g_j = 0$  for all  $j = 1, \dots, d$  which, in turn, implies that  $A^n g_j = 0$  and  $D_t A^n g_j = 0$  for all  $j = 1, \dots, d$  and  $n = 1, 2, \dots$ . Therefore, by equations (20)–(22) we have

$$\mu_{jk}^0 = \langle g_j, u_k \rangle_2, \quad \mu_{jk}^n = 0, \quad j, k = 1, \dots, d, \quad n = 1, 2, 3, \dots. \quad (36)$$

Let's first focus on the spectral measure  $\mu_{kk}$  for some  $k = 1, \dots, d$ , which is a *positive* measure. It's clear that the only positive Stieltjes measure with all moments having value zero is a  $\delta$ -measure concentrated at  $\lambda = 0$ ,  $\delta_0(d\lambda)$ , where  $\delta_a(d\lambda)$  is the  $\delta$ -measure concentrated at  $\lambda = a$ . We therefore have the following result regarding the positive measure  $\mu_{kk}$  for simple shear flow,

$$\mu_{kk} = \mu_{kk}^0 \delta_0(d\lambda). \quad (37)$$

We now show the signed measures  $\text{Re } \mu_{jk}$  and  $\text{Im } \mu_{jk}$ ,  $j \neq k$ , also satisfy (37) in a weak sense. By the Jordan decomposition theorem [9] there exist unique positive measures  $\text{Re } \mu_{jk}^+$  and  $\text{Re } \mu_{jk}^-$  such that

$\operatorname{Re} \mu_{jk} = \operatorname{Re} \mu_{jk}^+ - \operatorname{Re} \mu_{jk}^-$  and  $\operatorname{Re} \mu_{jk}^+ \perp \operatorname{Re} \mu_{jk}^-$ , and similarly for the signed measure  $\operatorname{Im} \mu_{jk}$ . This and (36) imply the moments of these measures satisfy

$$[\operatorname{Re} \mu_{jk}^+]^n = [\operatorname{Re} \mu_{jk}^-]^n, \quad [\operatorname{Im} \mu_{jk}^+]^n = [\operatorname{Im} \mu_{jk}^-]^n, \quad n = 1, 2, 3, \dots, \quad (38)$$

where  $[\operatorname{Re} \mu_{jk}^+]^n$  and  $[\operatorname{Re} \mu_{jk}^-]^n$  are the  $n$ th moments of the measures  $\operatorname{Re} \mu_{jk}^+$  and  $\operatorname{Re} \mu_{jk}^-$ , for example. Consequently, (36) implies for all polynomials  $P(\lambda)$  satisfying  $P(0) = 0$  that

$$\int_{\Sigma} P(\lambda) d\operatorname{Re} \mu_{jk}(\lambda) = 0, \quad j \neq k. \quad (39)$$

Since  $\operatorname{Re} \mu_{jk}^+ \perp \operatorname{Re} \mu_{jk}^-$ , it is clear that this can only be the case if  $\operatorname{Re} \mu_{jk} = \operatorname{Re} \mu_{jk}^0 \delta_0(d\lambda)$ . A similar argument establishes that  $\operatorname{Im} \mu_{jk} = \operatorname{Im} \mu_{jk}^0 \delta_0(d\lambda)$ . Hence, we have that

$$\mu_{jk} = \mu_{jk}^0 \delta_0(d\lambda), \quad j \neq k. \quad (40)$$

This argument can be strengthened for the setting of a time-independent fluid velocity field,  $\mathbf{u} = \mathbf{u}(\mathbf{x})$ . In this case, the self-adjoint operator  $M$  has bounded spectrum  $\Sigma \subseteq [-\|M\|, \|M\|]$  [20, 23]. The Stone Weierstrass theorem [9] then extends the result in (39) to functions  $\xi(\lambda)$  continuous on the closed interval  $[-\|M\|, \|M\|]$  satisfying  $\xi(0) = 0$ , thus (40) holds in this strengthened sense.

## 4.2 Moments for BC-flow

In this section we demonstrate how the iterative method developed in Section 3 can be used to compute an arbitrary number of moments for the spectral measure  $\mu_{jk}$  associated with *BC*-flow, which is given by the fluid velocity field [15]

$$\mathbf{u} = (C \cos y, B \cos x). \quad (41)$$

In particular, we implement the iterative method using Maple's symbolic math toolbox to calculate the mass  $\mu_{jk}^0$  and the moments  $\mu_{jk}^{2n}$ ,  $2n = 2, 4, \dots, 12$  analytically in closed form. We then discuss how higher order moments can be numerically computed to floating point precision.

In terms of the Fourier basis  $\{\phi_{m,n}\}$  for  $\mathcal{H}_V$  [9], where  $\phi_{m,n}(x, y) = \exp(i(mx + ny))$ , the components  $u_j$ ,  $j = 1, 2$ , of the fluid velocity field  $\mathbf{u} = (C \cos y, B \cos x)$  are given by

$$\begin{aligned} u_1 &= (C/2)(\phi_{0,1} + \phi_{0,-1}), \\ u_2 &= (B/2)(\phi_{1,0} + \phi_{-1,0}). \end{aligned} \quad (42)$$

From equations (26), (27), and (42) we have

$$g_j = u_j, \quad j = 1, 2. \quad (43)$$

The operator  $D_t = \mathbf{u} \cdot \nabla = u_1 \partial_x + u_2 \partial_y$  is given by

$$D_t = (C/2)[\phi_{0,1} + \phi_{0,-1}] \partial_x + (B/2)[\phi_{1,0} + \phi_{-1,0}] \partial_y. \quad (44)$$

Since  $\partial_x u_1 = 0$  and  $\partial_y u_2 = 0$ , equations (26) and (42)–(44) yield

$$\begin{aligned} D_t g_1 &= (C/2)(iB/2)(\phi_{1,1} + \phi_{-1,1} - \phi_{1,-1} - \phi_{-1,-1}), \\ D_t g_2 &= (B/2)(iC/2)(\phi_{1,1} + \phi_{1,-1} - \phi_{-1,1} - \phi_{-1,-1}). \end{aligned} \quad (45)$$

Since  $A = (-\Delta)^{-1} D_t$ , it follows from equations (26) and (45) that

$$A g_j = D_t g_j / 2, \quad j = 1, 2. \quad (46)$$

We now use equations (42)–(46) to compute the mass and the first two moments of the spectral measure  $\mu_{jk}$ . From equations (32) and (43) we have  $b_{m,n}^j = a_{m,n}^j$ , where  $a_{0,1}^1 = a_{0,-1}^1 = C/2$  and  $a_{1,0}^2 = a_{-1,0}^2 = B/2$ ,

Table 1: Exact values of the spectral measure moments  $\mu_{kk}^{2n}$  for BC- flow with fluid velocity field in equation (41) with  $B = C = 1$ , computed using Maple's symbolic math toolbox. Off-diagonal moments satisfy  $\mu_{jk}^{2n} = 0$ ,  $j \neq k$ .

and all other coefficients  $a_{m,n}^j = 0$ . Consequently, from equation (20),  $\mu_{jk}^0 = \langle g_j, u_k \rangle_2$ , or the first formula in (33),  $\mu_{jk}^0 = \sum_{m,n} b_{m,n}^j \bar{a}_{m,n}^k$ , we have

$$\mu_{11}^0 = \frac{C^2}{2}, \quad \mu_{22}^0 = \frac{B^2}{2}, \quad \mu_{12}^0 = 0. \quad (47)$$

Similarly, from the formulas in equation (21)  $\mu_{jk}^1 = -i \langle D_t g_j, g_k \rangle_2$  and  $\mu_{jk}^2 = \langle D_t g_j, A g_k \rangle_2$  or the last two formulas in equation (33),  $\mu_{jk}^1 = -i \sum_{\ell,k} c_{\ell,k}^j \bar{b}_{\ell,k}^k$ , and  $\mu_{jk}^2 = \sum_{\ell,k} c_{\ell,k}^j \bar{d}_{\ell,k}^k$ , we have  $\mu_{jk}^1 = 0$  and

$$\mu_{11}^2 = \mu_{22}^2 = \frac{B^2 C^2}{8}, \quad \mu_{12}^2 = 0. \quad (48)$$

While the calculations of the mass and the first two moments are quite transparent, calculations of higher order moments become complicated quickly. Analytical closed form expressions can be obtained using Maple's symbolic math toolbox. These calculations indicate that  $\mu_{12}^{2n} = 0$  for all  $2n = 0, 2, 4, 6, \dots$  and

$$\begin{aligned}\mu_{11}^4 &= (1/320)B^2C^4 + (11/320)B^4C^2, \\ \mu_{11}^6 &= \frac{3B^2C^2(101B^4 + 25B^2C^2 + C^4)}{32000}, \\ \mu_{11}^8 &= \frac{B^2C^2(567567B^6 + 233070B^4C^2 + 39610B^2C^4 + 617C^6)}{217600000}, \\ \mu_{11}^{10} &= \frac{C^2B^2(567567B^6 + 233070B^4C^2 + 39610B^2C^4 + 617C^6)}{217600000}, \\ \mu_{11}^{12} &= \frac{C^2B^2(3455217211B^8 + 1985186775B^6C^2 + 556637120B^4C^4 + 85049835B^2C^6 + 412611C^8)}{4808960000000},\end{aligned}\tag{49}$$

where  $\mu_{22}^{2n}$  as a function of  $B$  and  $C$ ,  $\mu_{22}^{2n}(B, C)$  satisfies  $\mu_{22}^{2n}(B, C) = \mu_{11}^{2n}(C, B)$ . We were able to calculate the moments  $\mu_{ij}^{2n}(B, C)$  for BC-flow in closed form up to  $2n = 26$  for arbitrary  $B, C \in (0, 1]$ , given the computational resources used. Some of these are displayed in Table 1 for  $B = C = 1$ .

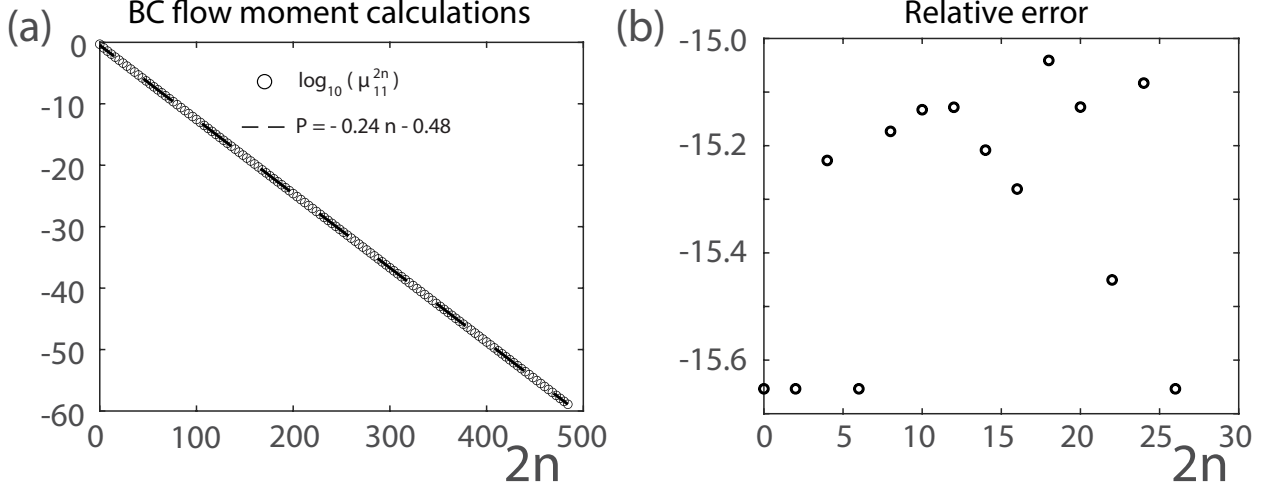


Figure 1: **Spectral measure moment computations for BC-cell-flow.** (a) Numerical computation of the moments  $\mu_{11}^{2n}$  displayed in log-10 scale for BC-flow in (41) with  $B = C = 1$  using the iterative scheme shown in equations (50)–(52). The linear fit to the data  $\log_{10}(\mu_{11}^{2n})$  suggests the power law behavior  $\mu_{11}^{2n} \sim 10^{-0.24(2n)}$  for  $n \gg 1$ . (b) Error of the floating point computations in (a) relative to the exact values, i.e.,  $|\mu_{\text{float}}^{2n} - \mu_{\text{exact}}^{2n}|/\mu_{\text{exact}}^{2n}$ , showing excellent agreement with error values  $\lesssim 10^{-15}$  for  $2n = 0, 2, \dots, 26$ .

Numerically computing higher order moments using floating point arithmetic can be accomplished using the mapping in equation (31) as follows. The action of the inverse Laplacian on a Fourier mode  $\phi_{m,n}(x, y) = \exp(i(mx + ny))$  is given by,

$$(-\Delta)^{-1}\phi_{m,n} = \phi_{m,n}/(m^2 + n^2), \quad m^2 + n^2 \neq 0. \quad (50)$$

Also, since  $\phi_{i,j}\phi_{k,l} = \phi_{i+k,j+l}$ , from equations (26) and (44) we have

$$D_t\phi_{m,n} = (imC/2)\phi_{m,n+1} + (imC/2)\phi_{m,n-1} + (inB/2)\phi_{m+1,n} + (inB/2)\phi_{m-1,n}, \quad m^2 + n^2 \neq 0, \quad (51)$$

with  $A\phi_{m,n} = (-\Delta)^{-1}D_t\phi_{m,n}$ . Equations (33) and (35) together with (50) and (51) define an iterative method that can be used to compute Fourier coefficients for the functions in the iterative mapping chain:

$$u_j \mapsto g_j \mapsto D_t g_j \mapsto Ag_j \mapsto D_tA g_j \mapsto A^2 g_j \mapsto D_t A^2 g_j \mapsto A^3 g_j \mapsto \dots \quad (52)$$

This can be used to numerically compute an arbitrary number of moments  $\mu_{jk}^n$  for BC-flow, the maximum number limited only by numerical accuracy and computational resources.

We have used this iterative method to calculate hundreds of spectral measure moments  $\mu_{11}^{2n}$  for BC-cell-flow with fluid velocity field in equation (41) and  $B = C = 1$  using Matlab — shown in Fig. 1. Since the operator  $A$  is bounded for this 2D steady flow, the moments decrease exponentially for large  $n$ , and Fig. 1(a) suggests the power law behavior  $\mu_{11}^{2n} \sim 10^{-0.24(2n)}$  for  $n \gg 1$ . Fig. 1(b) shows the error of the computed values of  $\mu_{11}^{2n}$  using Matlab, relative to the exact values in Table 1, with error values  $\lesssim 10^{-15}$  indicating quite accurate numerical computation of the  $\mu_{11}^{2n}$ .

### 4.3 Moments for a 2D time-periodic flow

In this section we demonstrate how the iterative method developed in Section 3 can be used to compute an arbitrary number of moments for the spectral measure  $\mu_{jk}$  associated with the space-time periodic flow [15, 5]

$$\mathbf{u} = (C \cos y, B \cos x) + \theta \cos t (\sin y, \sin x). \quad (53)$$

In particular, we implement the iterative method using Maple's symbolic math toolbox to calculate the first few moments analytically in closed form. We then demonstrate how higher order moments can be numerically computed to floating point precision.

Dynamic BC flow		
$2n$	$\mu_{kk}^{2n}$	$\mu_{jk}^{2n}$
0	$3/4$	0
2	$35/64$	0
4	$1069/1280$	$5/32$
6	$282223/163840$	$473/800$
8	$15778075321/3481600000$	$83952089/51200000$

Table 2: Exact values of the spectral measure moments  $\mu_{kk}^{2n}$  and  $\mu_{jk}^{2n}$ ,  $j \neq k$ , for the fluid velocity field in equation (53) with  $B = C = \theta = 1$ , calculated using Maple's symbolic math toolbox.

Denote  $\mathbf{u} = \mathbf{u}_{BC} + \mathbf{u}_\theta$ , where  $\mathbf{u}_{BC} = (C \cos y, B \cos x)$  is the fluid velocity field in equation (42) and  $\mathbf{u}_\theta = \theta \cos t (\sin y, \sin x)$ . The components  $u_j$ ,  $j = 1, 2$ , of the fluid velocity field  $\mathbf{u}$  in (53) expressed in terms of the Fourier basis  $\{\phi_{\ell,m,n}\}$  for  $\mathcal{HTV}$  [9], where  $\phi_{\ell,m,n}(x, y, t) = \exp(i(\ell t + mx + ny))$ , are given by

$$\begin{aligned} [\mathbf{u}_{BC}]_1 &= (C/2)(\phi_{0,0,1} + \phi_{0,0,-1}), \\ [\mathbf{u}_{BC}]_2 &= (B/2)(\phi_{0,1,0} + \phi_{0,-1,0}), \\ [\mathbf{u}_\theta]_1 &= (\theta/4i)(\phi_{1,0,1} + \phi_{-1,0,1} - \phi_{1,0,-1} - \phi_{-1,0,-1}), \\ [\mathbf{u}_\theta]_2 &= (\theta/4i)(\phi_{1,1,0} + \phi_{-1,1,0} - \phi_{1,-1,0} - \phi_{-1,-1,0}). \end{aligned} \quad (54)$$

Writing  $\mathbf{g} = \mathbf{g}_{BC} + \mathbf{g}_\theta$  with  $\mathbf{g} = (-\Delta)^{-1}\mathbf{u}$ , using the notation that  $(-\Delta)^{-1}$  operates component-wise on  $\mathbf{u}$ , we have from (54)

$$\mathbf{g} = \mathbf{u}_{BC} + \mathbf{u}_\theta. \quad (55)$$

In this time-independent setting,  $D_t = \partial_t + \mathbf{u} \cdot \nabla$ , hence by linearity

$$D_t = \partial_t + \mathbf{u}_{BC} \cdot \nabla + \mathbf{u}_{bc} \cdot \nabla. \quad (56)$$

From equation (26), we have

$$\partial_t \phi_{\ell,m,n} = i\ell \phi_{\ell,m,n}, \quad \ell \neq 0. \quad (57)$$

We have the following analogue of equation (51), for  $m^2 + n^2 \neq 0$ ,

$$\mathbf{u}_{BC} \cdot \nabla \phi_{\ell,m,n} = (imC/2) \phi_{\ell,m,n+1} + (imC/2) \phi_{\ell,m,n-1} + (inB/2) \phi_{\ell,m+1,n} + (inB/2) \phi_{\ell,m-1,n}. \quad (58)$$

From equation (54) we have, for  $m^2 + n^2 \neq 0$ ,

$$\begin{aligned} \mathbf{u}_\theta \cdot \nabla \phi_{\ell,m,n} &= (imc/4i) \phi_{\ell+1,m,n+1} + (imc/4i) \phi_{\ell-1,m,n+1} - (imc/4i) \phi_{\ell+1,m,n-1} \\ &\quad - (imc/4i) \phi_{\ell-1,m,n-1} + (inb/4i) \phi_{\ell+1,m+1,n} + (inb/4i) \phi_{\ell-1,m+1,n} \\ &\quad - (inb/4i) \phi_{\ell+1,m-1,n} - (inb/4i) \phi_{\ell-1,m-1,n}. \end{aligned} \quad (59)$$

Similarly, we have the following analogue of equation (50)

$$(-\Delta)^{-1} \phi_{\ell,m,n} = \phi_{\ell,m,n} / (m^2 + n^2) \quad m^2 + n^2 \neq 0. \quad (60)$$

Equations (33) and (35) together with equations (58)–(60) enable all the Fourier coefficients in the iterative sequence shown in equation (52) to be obtained analytically in closed form.

Using Maple's symbolic math toolbox, this yields the spectral measure masses

$$\mu_{11}^0 = \frac{C^2}{2} + \frac{\theta^2}{4}, \quad \mu_{22}^0 = \frac{B^2}{2} + \frac{\theta^2}{4}, \quad \mu_{12}^0 = 0. \quad (61)$$

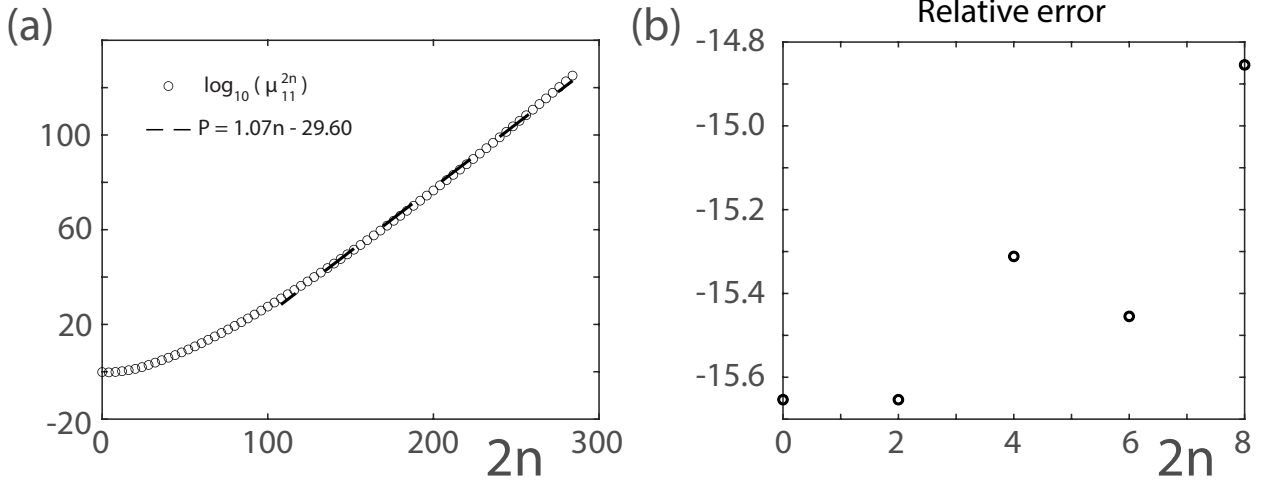


Figure 2: **Spectral measure moment computations for a 2D time-periodic flow.** (a) Numerical computation of moments  $\mu_{11}^{2n}$  displayed in log-10 scale for the time-periodic flow in (53) with  $B = C = \theta = 1$  using the iterative scheme shown in equations (57)–(60). The linear fit to the data  $\log_{10}(\mu_{11}^{2n})$  suggests the power law behavior  $\mu_{11}^{2n} \sim 10^{1.07(2n)}$  for  $n \gg 1$ . (b) Error of the numerical moment computations in (a) relative to the exact values, showing excellent agreement with error values  $\lesssim 10^{-14.8}$  for  $2n = 0, 2, 4, 6, 8$ .

Recall that all odd moments are identically zero. The second, fourth, and sixth moments are given by

$$\begin{aligned}
\mu_{11}^2 &= \frac{3\theta^4}{64} + \frac{(B^2 + C^2 + 4)\theta^2}{16} + \frac{B^2C^2}{8}, \\
\mu_{12}^2 &= 0, \\
\mu_{11}^4 &= \frac{5\theta^6}{3072} + \frac{(323B^2 + 705C^2 + 1090)\theta^4}{92160} + \frac{(180 + 22B^4 + (366C^2 + 245)B^2 + 8C^4 + 80C^2)\theta^2}{11520} \\
&\quad + \frac{11B^4C^2}{320} + \frac{C^4B^2}{320}, \\
\mu_{12}^4 &= -\frac{13BC\theta^4}{5760} - \left( \frac{18(B^3C + BC^3) + 35BC}{11520} \right) \theta^2, \\
\mu_{11}^6 &= \frac{20701\theta^8}{49152000} + \left( \frac{31583}{4608000} + \frac{4861B^2}{3686400} + \frac{3119C^2}{1228800} \right) \theta^6 + \left( \frac{49}{2304} + \frac{163871B^2}{9216000} + \frac{4343B^4}{3072000} \right. \\
&\quad \left. + \frac{48329C^2}{3072000} + \frac{108793B^2C^2}{9216000} + \frac{161C^4}{204800} \right) \theta^4 + \left( \frac{1}{64} + \frac{337B^2}{9216} + \frac{33191B^4}{2304000} + \frac{101B^6}{192000} + \frac{C^2}{576} \right. \\
&\quad \left. - \frac{2569B^2C^2}{2304000} + \frac{773B^4C^2}{48000} + \frac{11C^4}{16000} + \frac{137B^2C^4}{36000} + \frac{C^6}{48000} \right) \theta^2 + \frac{303B^6C^2}{32000} + \frac{3B^4C^4}{1280} + \frac{3B^2C^6}{32000}, \\
\mu_{12}^6 &= \frac{437BC\theta^6}{4608000} + \left( \frac{6509BC}{1536000} + \frac{521B^3C}{576000} + \frac{521BC^3}{576000} \right) \theta^4 + \left( \frac{65BC}{9216} - \frac{12841B^3C}{2304000} - \frac{9B^5C}{32000} - \frac{12841BC^3}{2304000} \right. \\
&\quad \left. + \frac{91B^3C^3}{28800} - \frac{9BC^5}{32000} \right) \theta^2,
\end{aligned} \tag{62}$$

where  $\mu_{22}^{2n}$  as a function of  $B$ ,  $C$ , and  $\theta$ ,  $\mu_{22}^{2n}(B, C, \theta)$  satisfies  $\mu_{22}^{2n}(B, C, \theta) = \mu_{11}^{2n}(C, B, \theta)$ . Exact rational values for  $2n = 0, 2, \dots, 8$  are displayed in Table 2 for  $B = C = \theta = 1$ .

We have used this iterative method to calculate hundreds of spectral measure moments  $\mu_{11}^{2n}$  for the 2D time-periodic fluid velocity field in equation (53) with  $B = C = \theta = 1$  using Matlab — shown in Fig. 2. Since the operator  $A$  is unbounded for this time-periodic flow, the moments increase exponentially for large  $n$ , and Fig. 2(a) suggests the power law behavior  $\mu_{11}^{2n} \sim 10^{0.54(2n)}$  for  $n \gg 1$ . Fig. 1(b) shows the error of the numerically computed values of  $\mu_{11}^{2n}$  using Matlab relative to the exact values in Table 2, with error values  $\lesssim 10^{-14.8}$  indicating quite accurate numerical computation of the  $\mu_{11}^{2n}$ .

## 5 Bounds for effective diffusivity

In the advection dominated regime, where  $\varepsilon \ll 1$ , it is known [6] that the asymptotic behavior of the effective diffusivity for BC-cell flow discussed in Section 4.2 is given by  $\mathfrak{D}_{kk}^* \sim \varepsilon^{1/2}$  as  $\varepsilon \rightarrow 0$ . The physical idea for this vanishing behavior of  $\mathfrak{D}_{kk}^*$  as  $\varepsilon \rightarrow 0$  is as follows. For  $\varepsilon = 0$ , passive tracers are trapped in closed streamlines of the cell flow [16, 15] and without the presence of molecular diffusivity  $\varepsilon$  there can be no large scale, macroscopic transport. However, for  $\varepsilon > 0$ , molecular diffusion can move tracers to neighboring streamlines and ultimately to neighboring period cells, giving rise to macroscopic transport on large spatial scales, with  $\mathfrak{D}_{kk}^* \sim \varepsilon^{1/2}$  as  $\varepsilon \rightarrow 0$ . In [5] it was conjectured that, due to the chaotic dynamics of the time-dependent fluid velocity field  $\mathbf{u}$  in (53), the effective diffusivity  $\mathfrak{D}_{kk}^*$  has the asymptotic behavior  $\mathfrak{D}_{kk}^* \sim 1$  for  $\varepsilon \ll 1$ , which is a phenomenon known as residual diffusivity.

Both of the asymptotic behaviors  $\mathfrak{D}_{kk}^* \sim \varepsilon^{1/2}$  for BC-flow and  $\mathfrak{D}_{kk}^* \sim 1$  for the dynamic flow in (53) were numerically verified in [15, 16]. This was accomplished in [15] by developing Fourier methods for computing the effective diffusivity  $\mathfrak{D}_{kk}^*$  by directly computing the spectral measure  $\mu$ . The cell problem in equation (17) was represented as an infinite system of equations involving the Fourier coefficients of the fluid velocity field  $\mathbf{u}$ . Truncating the system of equations results in a Hermitian matrix representation for the operator  $M = -iA$  in equations (17) and (18). The spectral measure of the matrix is given by a finite sum of weighted Dirac- $\delta$  functions  $d\mu(\lambda) = \sum_i m_i \delta_{\lambda_i}(d\lambda)$ , for  $i = 0, 1, 2, \dots$ . Here, the spectral weights  $m_i$  are given explicitly in terms of the eigenvectors of the matrix and  $\lambda_i$  are the eigenvalues of the matrix.

In this section, we describe these and other phenomena in terms of Padé approximants of the diagonal coefficients  $\mathfrak{D}_{kk}^*$ ,  $k = 1, \dots, d$ , of the effective diffusivity matrix which involve the moments  $\mu_{kk}^n$  of the *positive* measure  $\mu_{kk}$ . For simplicity, let's focus on one diagonal coefficient and set  $\mu_{kk}^n = \mu^n$ . With this notation, equation (19) can be written as  $\mathfrak{D}_{kk}^* = \varepsilon(1 + \varepsilon^{-2}f(\varepsilon^{-2}))$ , where  $f(z)$  is a *Stieltjes function* [3] of the variable  $z = \varepsilon^{-2}$  involving the positive measure  $\mu$ .

Padé approximants  $\{[N-1/N]\}_{N=1}^\infty$  and  $\{[N/N]\}_{N=1}^\infty$  form rigorous, converging lower and upper bounds for the Stieltjes function  $f(z)$  [3]

$$[N-1/N](z) \leq f(z) \leq [N/N](z), \quad f(z) = \int_{-\infty}^{\infty} \frac{d\mu(\lambda)}{1+z\lambda^2}. \quad (63)$$

Since all of the terms of the expression in  $\mathfrak{D}_{kk}^* = \varepsilon(1 + \varepsilon^{-2}f(\varepsilon^{-2}))$  are positive, we therefore have the following rigorous lower and upper bounds for  $\mathfrak{D}_{kk}^*$

$$\varepsilon(1 + \varepsilon^{-2}[N-1/N](\varepsilon^{-2})) \leq \mathfrak{D}_{kk}^*(\varepsilon) \leq \varepsilon(1 + \varepsilon^{-2}[N/N](\varepsilon^{-2})). \quad (64)$$

The theory of Padé approximants for  $f(z)$  follows by expanding  $1/(1+z\lambda^2)$  in a geometric series and writing  $f(z)$  as a *series of Stieltjes*

$$f(z) = \sum_{n=0}^{\infty} c_n z^n, \quad c_n = (-1)^n \mu^{2n}, \quad \mu^n = \int_{-\infty}^{\infty} \lambda^n d\mu(\lambda). \quad (65)$$

The  $L, N$  Padé approximant of  $f(z)$  is given by

$$[L/N](z) = \frac{P^{[L/N]}(z)}{Q^{[L/N]}(z)}, \quad (66)$$

where  $P^{[L/N]}(z)$  is a polynomial of degree of at most  $L$  and  $Q^{[L/N]}(z)$  is a polynomial of degree of at most  $N$ . The *formal* power series for  $f(z)$  in equation (65) and the condition  $f(z) - P^{[L/N]}(z)/Q^{[L/N]}(z) = O(z^{L+N+1})$  determines the coefficients of  $P^{[L/N]}(z)$  and  $Q^{[L/N]}(z)$  and these polynomials can be written in terms of determinants involving the  $c_n$  [3].

### 5.1 Numerical implementation

Given the moments  $\mu^{2n}$  obtained in Section 4.3, it might seem that Padé approximants for  $\mathfrak{D}_{kk}^*$  of any order could be attainable. However, even in the absence of rounding errors on a computer, the theoretical treatment of Padé approximants is subject to the appearance of seemingly spurious pole-zero pairs or “Froissart

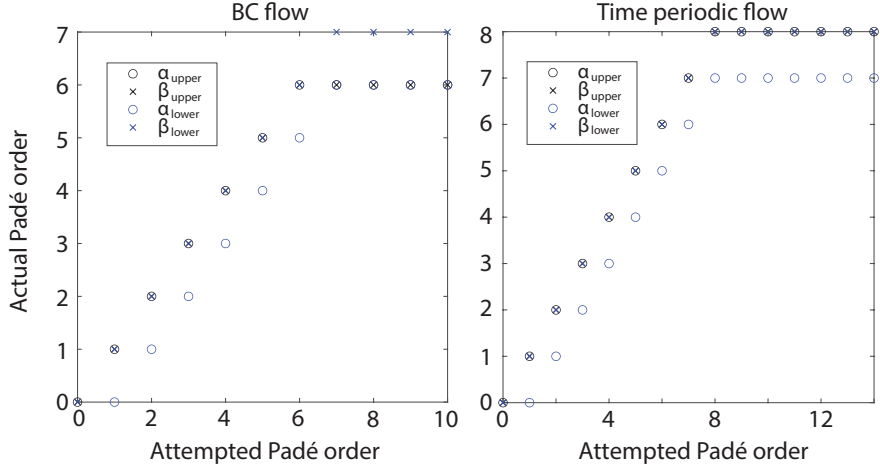


Figure 3: **Padé bound orders for effective diffusivity.** Attempted and actual numerator and denominator polynomial orders for  $[N/N]$  upper and  $[N - 1/N]$  lower bounds for various values of  $N$ . These bounds for Stieltjes functions associated with the effective diffusivity  $\mathfrak{D}_{kk}^*$  are for (a) BC-flow and (b) 2D time-periodic flow with fluid velocity fields in equations (41) and (53). The actual numerator and denominator polynomial orders returned for the attempted  $[N/N]$  upper and  $[N - 1/N]$  lower bounds are  $[\alpha_{upper}/\beta_{upper}]$  and  $[\alpha_{lower}/\beta_{lower}]$ .

doublets” in arbitrary locations that prevent pointwise convergence [10]. Such anomalies become common in the presence of rounding errors or other forms of noise [10]. Hence, computing the Padé approximants directly in terms of the determinants is essentially ill-posed and becomes unreliable for large polynomial degree. Padé approximation uses information about the series of Stieltjes  $f(z)$  in (65) at a single point  $z = 0$  in the complex plane to gain information about regions of the complex plane away from  $z = 0$  — similar to analytic continuation — and becomes more ill-posed further away from  $z = 0$ . This is a fundamental limitation of using Padé approximant bounds to study the effective diffusivity in the advection dominated regime, where  $\varepsilon \ll 1$ , i.e.,  $z \gg 1$ . Despite this, we will show for the case of BC-flow that Padé approximants capture the known asymptotic behavior  $\mathfrak{D}_{kk}^* \sim \varepsilon^{1/2}$  for  $\varepsilon \gg 1$  [6].

Such issues associated with numerical computation of Padé approximants are addressed in [10], where a Matlab function `padeapprox` was released, which is freely available as part of `Chebfun`, which provides robust Padé approximants via singular value decomposition (SVD) [10]. This numerical method does not enable Padé approximants of an arbitrary order to be computed, but instead truncates the Padé approximants to an order that ensures numerical stability, hence numerically dependable results — incorporating any additional moments typically results in the same truncated Padé order. This automatic truncation is accomplished by introducing a tolerance `tol` that is used to zero out singular values less than `tol`. For most purposes involving problems perturbed just by rounding errors,  $tol = 10^{-14}$  is a reasonable value [10]. This regularization can be circumvented by setting `tol=0` [10]. The desired degrees of the numerator/denominator polynomials, in our case  $N/N$  and  $N - 1/N$ , are provided along with a vector of the coefficients  $c_n$  and `tol`; Numerator and denominator polynomials of actual degree  $\alpha$  and  $\beta$  are returned, as shown in Figure 3.

The numerical computation of Padé approximants can be further stabilized by scaling the  $c_n$  in (65) by picking a  $\gamma > 0$  so that  $f(z) = \sum_n (c_n \gamma^n) (z/\gamma)^n$  has scaled coefficients  $c_n \gamma^n$ . The goal is to obtain scaled coefficients that have roughly comparable orders of magnitude, neither decreasing nor increasing at a rapid geometric rate, for which the algorithm `padeapprox` is most effective [10]. Figure 4a shows this rescaling is effective for BC-flow, with the variation in the moments decreasing from  $\sim 7$  orders of magnitude to  $\sim 1$  order of magnitude. Figure 4b shows the moment scaling for the time-periodic flow is less effective but does decrease the variation in the moments from  $\sim 14$  orders of magnitude to  $\sim 10$  orders of magnitude. Once Padé approximants are calculated using these scaled moments the original approximants are recovered by simply using the scaled parameter  $z \mapsto z/\gamma$ .

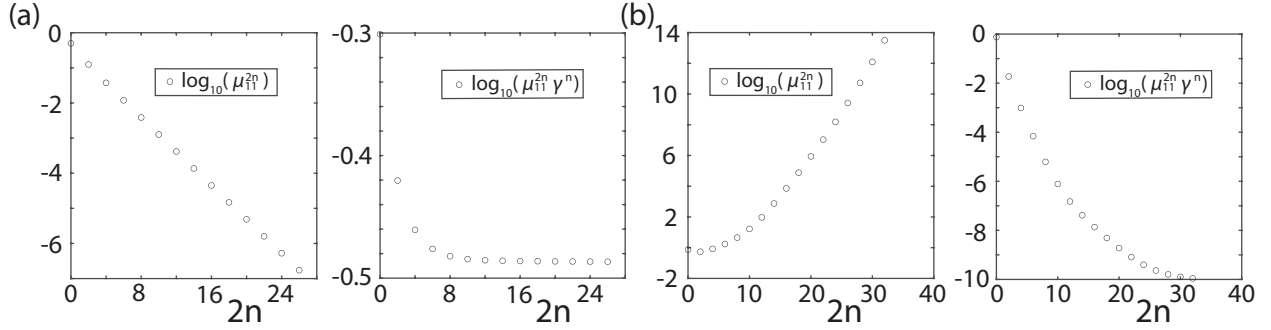


Figure 4: **Scaled spectral measure moments.** Unscaled and scaled spectral measure moments for (a) BC-flow and (b) space-time periodic flow. (a) The scaled moments  $\mu_{11}^{2n}\gamma^n$  for BC-flow with  $\gamma = 3.0387$  reduces the variation of the moments from  $\sim 7$  orders of magnitude to  $\sim 1$  order of magnitude. (b) The scaled moments  $\mu_{11}^{2n}\gamma^n$  for space-time periodic flow with  $\gamma = 0.0342$  reduces the variation of the moments from  $\sim 14$  orders of magnitude to  $\sim 10$  orders of magnitude.

## 5.2 Bounds for BC-flow

In this section we discuss our results for Padé approximant upper  $[N/N]$  and lower  $[N-1/N]$  bounds for the effective diffusivity  $\mathfrak{D}_{kk}^*$  for BC-flow with fluid velocity field given in equation (41). In particular, we incorporated into the Matlab function `padeapprox` the moments  $\mu^{2n}$ ,  $2n = 0, \dots, 26$ , for the spectral measure  $\mu$  for BC-cell-flow with  $B = C = 1$ . Figures 5(a) and (b) display, in linear and log-log scale respectively, progressively higher order Padé approximants  $[N/N]$  and  $[N-1/N]$  for the effective diffusivity  $\mathfrak{D}_{kk}^*$  as a function of  $\varepsilon$  for  $N = 1, \dots, 7$ . Here, the maximum order  $N = 7$  corresponds to the upper  $[6/6]$  and lower  $[6/7]$  Padé approximants due to the truncation which occurs as illustrated in Figure 3(a). From  $\mathfrak{D}_{kk}^* = \varepsilon(1 + \varepsilon^{-2}f(\varepsilon^{-2}))$  with  $f \geq 0$  we see the global lower bound is  $\mathfrak{D}_{kk}^* \geq \varepsilon$ , which is shown in Figures 5(a) and (b) in black-dash line style. The global upper bound is attained by shear flow [2], discussed in Section 4.1, where the spectral measure is given by a delta measure at the spectral origin,  $\mu = \mu^0 \delta_0(d\lambda)$ , yielding the global upper bound  $\mathfrak{D}_{kk}^* \leq \varepsilon(1 + \mu^0/\varepsilon^2)$ , also shown in Figures 5(a) and (b) in black-dash line style. The difference  $[N/N] - [N-1/N]$  of upper and lower bounds are displayed in Figure 5(c), showing that the bounds are quite accurate for large  $\varepsilon$ , i.e., small  $z$ , and they become less accurate as  $\varepsilon \rightarrow 0$ , as anticipated and discussed in Section 5.1.

The bounds in Figures 5(a) and (b) get progressively tighter with increasing  $N$ , as indicated by the bound differences in Figure 5(c). Figures 5(a), (b), and (c) show that for  $\varepsilon \gtrsim 1$  all the bounds but the global upper and lower bounds lie virtually right on top of each other. The highest order bounds shown in Figure 5 incorporate the moments  $2n = 0, \dots, 24$  and  $2n = 0, \dots, 26$  for the upper and lower bounds, respectively. They capture the behavior of  $\mathfrak{D}_{kk}^*$  in the advection dominated regime where  $\varepsilon \ll 1$ . Linear polynomial fits to the bounds  $[6/6]$  and  $[6/7]$  in log-log scale capture the asymptotic behavior of the effective diffusivity  $\mathfrak{D}_{kk}^* \sim \varepsilon^{1/2}$  discussed in Section 5, with estimated critical exponents 0.49916 and 0.50166, respectively, as shown in Figure 5(d). The bound differences shown in Figure 5(c) indicate that the highest order bounds are accurate to within 0.01 for  $\varepsilon \gtrsim 0.053$  and within 0.1 for  $\varepsilon \gtrsim 0.025$  with  $\mathfrak{D}_{kk}^*(0.053) \approx 0.35$  and  $\mathfrak{D}_{kk}^*(0.025) \approx 0.24$  — demonstrating  $\approx 6.6$  and  $\approx 9.6$  times the enhancement of the effective diffusivity above  $\varepsilon$  even for the small values of  $\varepsilon = 0.053$  and  $\varepsilon = 0.025$ , respectively.

When more than  $2n = 26$  moments are supplied to the function `padeapprox`, in order to ensure numerical accuracy and stability, the function just truncates the Padé order to  $N = 7$ , as shown in Figure 3(a); supplying more moments just leads to the same repeated maximum order  $N = 7$  of the Padé bounds. A tolerance value `tol=10^-14` was used for all bounds in Figure 5. Reducing this value does lead to bounds of a higher order than  $N = 7$  when more moments than  $2n = 26$  are supplied, at the expense of numerical accuracy of the Padé bounds.

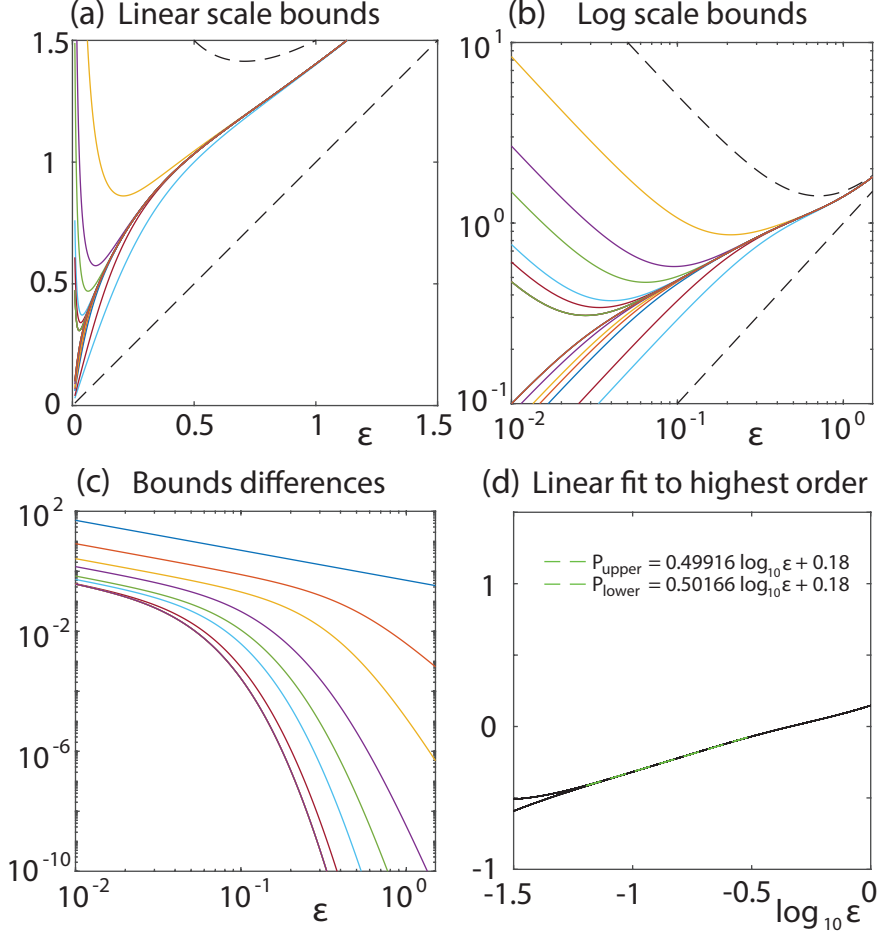


Figure 5: **Effective diffusivity bounds for BC-flow.** Padé approximant upper  $[N/N]$  and lower  $[N-1/N]$  bounds for  $\mathfrak{D}_{kk}^*(\varepsilon)$  as a function of  $\varepsilon$  for  $N = 1, \dots, 7$  in (a) linear scale and (b) log-log scale. (c) Differences of upper and lower bounds  $[N/N] - [N-1/N]$  for various values of  $N$  in log-log scale. (d) Linear polynomial fits to the highest order upper and lower bounds with  $N = 7$  demonstrating the asymptotic behavior  $\mathfrak{D}_{kk}^* \sim \varepsilon^{1/2}$  as  $\varepsilon \rightarrow 0$ .

### 5.3 Bounds for space-time periodic flow

In this section we discuss our results for Padé approximant upper  $[N/N]$  and lower  $[N-1/N]$  bounds for the effective diffusivity  $\mathfrak{D}_{kk}^*$  for the space-time periodic flow with fluid velocity field given in equation (53) with  $B = C = \theta = 1$ . In particular, we incorporated into the Matlab function `padeapprox` the moments  $\mu^{2n}$ ,  $2n = 0, \dots, 32$ , for the associated spectral measure  $\mu$ . Similar to Figure 5, Figures 6(a) and (b) display progressively higher order Padé approximants  $[N/N]$  and  $[N-1/N]$  for the effective diffusivity  $\mathfrak{D}_{kk}^*$  as a function of  $\varepsilon$ , with global lower and upper bounds displayed in black-dash line style.

The bounds in Figures 6(a) and (b) get progressively tighter with increasing  $N$ . For  $\varepsilon \gtrsim 1$  all bounds but the global upper and lower bounds lie virtually right on top of each other, as demonstrated quantitatively by the bound differences in Figure 6(c). The highest order bounds shown in Figure 6 correspond to  $N = 8$  which incorporates the moments  $2n = 0, \dots, 32$ . Figure 6(c) indicates the highest order bounds are accurate within a difference of 0.01 for  $\varepsilon \gtrsim 0.59$  and within a difference of 0.1 for  $\varepsilon \gtrsim 0.36$  with  $\mathfrak{D}_{kk}^*(0.59) \approx 1.22$  and  $\mathfrak{D}_{kk}^*(0.36) \approx 1.06$ , indicating  $\approx 2.07$  and  $\approx 2.94$  times the enhancement of the effective diffusivity above  $\varepsilon$  when  $\varepsilon = 0.59$  and  $\varepsilon = 0.36$ , respectively.

Comparing this to the value of the effective diffusivity for BC-flow for  $\varepsilon = 0.59$  and  $\varepsilon = 0.36$  shows the addition of the time dependent term  $\mathbf{u}_\theta = \theta \cos t (\sin y, \sin x)$  with  $\theta = 1$  leads to a  $\approx 5\%$  and  $\approx 16\%$

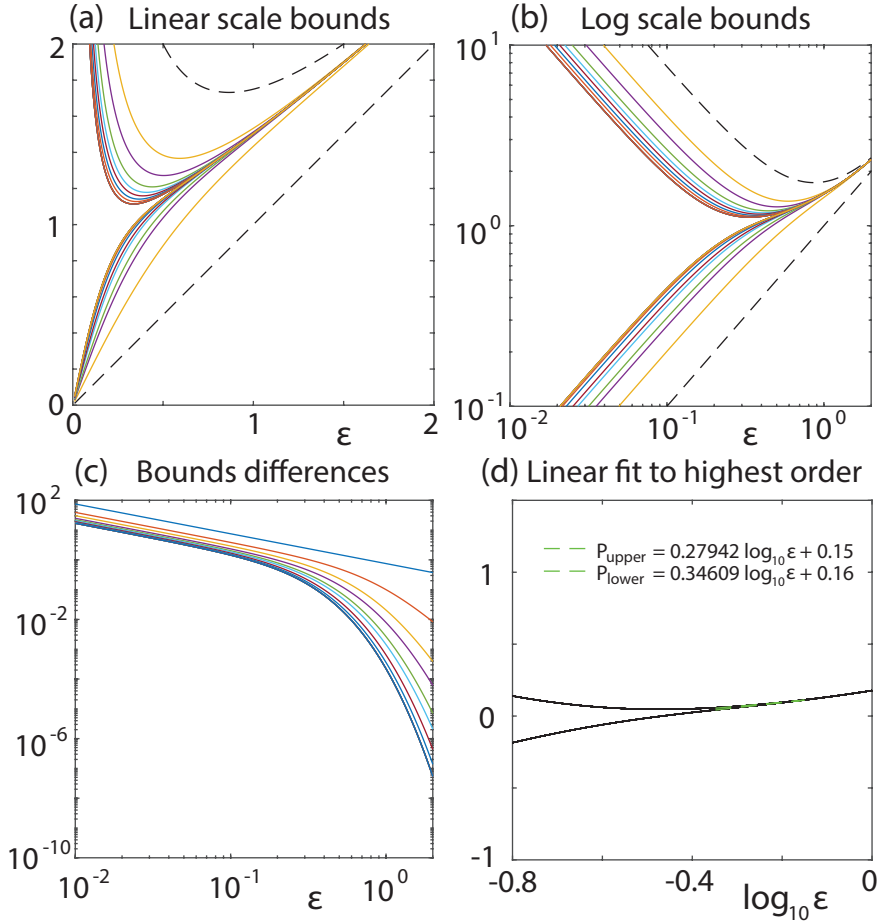


Figure 6: **Effective diffusivity bounds for space-time periodic flow.** Padé approximant upper [ $N/N$ ] and lower [ $N - 1/N$ ] bounds for  $N = 1, \dots, 8$  in linear scale (a) with corresponding absolute differences (b), and upper and lower bounds in log-log scale (c) in the variable  $\varepsilon$ . (d) Linear polynomial fits to the highest order upper and lower bounds with  $N = 8$ .

increase in the effective diffusivity, respectively — hence an even greater enhancement above the molecular diffusivity value. In [5, 15] numerical results indicate the addition of the time dependent term gives rise to an additional  $\mathfrak{D}_{kk}^*$  enhancement of  $\approx 10^{1.5}$  times that for BC-flow when  $\varepsilon \approx 10^{-4}$ , with  $\mathfrak{D}_{kk}^*$  flattening out into a  $\mathfrak{D}_{kk}^* \sim 1$  behavior for  $\varepsilon \approx 0.1$  with  $\mathfrak{D}_{kk}^*(10^{-4}) \approx 10^{-1/2}$ , compared to  $\mathfrak{D}_{kk}^*(10^{-4}) \approx 10^{-2}$  for BC-flow.

## 6 Conclusions

The effective diffusivity  $\mathfrak{D}^*$  associated with both spatially and space-time periodic fluid flows has a Stieltjes function representation involving a spectral measure  $\mu$  of a self-adjoint operator and the Péclet number  $Pe$  of the flow. We considered a non-dimensionalization that *separates* the geometry and dynamics of the fluid velocity field — encoded in  $\mu$  — from the strength of the fluid velocity field in  $Pe$ , which leads to the following simple relationship between the molecular diffusivity  $\varepsilon$  and  $Pe$ :  $Pe = 1/\varepsilon$ . The theory of Padé approximants for Stieltjes functions provides rigorous nested upper and lower bounds for  $\mathfrak{D}^*$  that incorporate the moments of  $\mu$ . The parameter separation property makes  $\mu$  and the bounds independent of the geometry and dynamics of the fluid velocity field. As more moments are incorporated the bounds get tighter and can converge to the true value of  $\mathfrak{D}^*$  for certain values of  $Pe$  near  $Pe = 0$ . Fundamental theoretical and numerical limitations of calculating Padé approximants far away from  $Pe = 0$  limit the accuracy of bounds for  $\mathfrak{D}^*$  in the advection dominated regime, where  $Pe \gg 1$ , i.e.,  $\varepsilon \ll 1$ . These limitations also limit the number of bounds that can

be stably computed.

An iterative method was introduced that enables an arbitrary number of moments of  $\mu$  to be calculated. This method was implemented in Maple to calculate several moments of both a steady and space-time periodic flow, in closed form as a function of flow parameters. This method was also implemented in Matlab to compute hundreds of moments to floating point precision, having excellent agreement with the exact values. These moments were incorporated into an existing numerical algorithm `padeapprox` [10] which computes Padé approximants in a robust, stable way.

Despite the fundamental limitations of calculating Padé approximants far away from  $Pe = 0$ , for the steady cell flow, BC-cell-flow, the known [6, 7] asymptotic behavior  $\mathfrak{D}^* \sim \varepsilon^{1/2}$ , for  $\varepsilon \ll 1$ , in the advection dominated regime was accurately captured by high order upper and lower bounds for  $\mathfrak{D}^*$ , for values of  $\varepsilon$  down to  $\varepsilon \approx 0.053$ . Bound differences for these highest order bounds indicate  $\mathfrak{D}^*$  was accurately computed within 0.01 for  $\varepsilon \gtrsim 0.053$  and within 0.1 for  $\varepsilon \gtrsim 0.025$ .

For the space-time periodic flow, which is BC-cell-flow with an additional space-time periodic term, the operator underlying the spectral measure  $\mu$  is *unbounded* which makes the computation of Padé approximant bounds for  $\mathfrak{D}^*$  less stable than the bounds for BC-cell-flow. This restricted our analysis of  $\mathfrak{D}^*$  in the advection dominated regime. Bound differences for the highest order bounds indicate the bounds are accurate to within 0.01 for  $\varepsilon \gtrsim 0.59$  and within 0.1 for  $\varepsilon \gtrsim 0.36$ . Comparing the values of  $\mathfrak{D}^*$  for BC-cell-flow and the space-time periodic flow for  $\varepsilon = 0.59$  and  $\varepsilon = 0.36$  shows the addition of the time dependent term to BC-cell-flow leads to a  $\approx 5\%$  and  $\approx 16\%$  increase in  $\mathfrak{D}^*$ , respectively.

The bounds for  $\mathfrak{D}^*$  for the space-time periodic flow are not accurate for small enough  $\varepsilon$  to capture the *residual diffusivity* phenomenon suggested by direct numerical computations of  $\mathfrak{D}^*$ . In particular, in [5, 15] numerical results indicate the addition of the time dependent term to BC-cell-flow gives rise to an additional  $\mathfrak{D}^*$  enhancement of  $\approx 10^{1.5} \approx 31.62$  times that for BC-cell-flow when  $\varepsilon \approx 10^{-4}$ , with  $\mathfrak{D}^*$  flattening out into a  $\mathfrak{D}^* \sim 1$  behavior when  $\varepsilon \lesssim 0.1$  with  $\mathfrak{D}_{kk}^*(10^{-4}) \approx 10^{-1/2}$ , compared to  $\mathfrak{D}_{kk}^*(10^{-4}) \approx 10^{-2}$  for BC-flow.

The iterative moment method developed in this manuscript enables analytic calculation of the moments of  $\mu$  in closed form for a large class of fluid velocity fields  $\mathbf{u}$ , namely spatially and space-time periodic  $\mathbf{u}$  with finite Fourier series, which are dense in the associated spaces of square integrable periodic functions [9]. This and the theory of Padé approximants for Stieltjes functions provide a remarkable advance in estimating the effective diffusivity, even in the advection dominated regime where  $\varepsilon$  is small for some  $\mathbf{u}$ .

## 7 Acknowledgements

We gratefully acknowledge support from the Applied and Computational Analysis Program and the Arctic and Global Prediction Program at the US Office of Naval Research through grants N00014-18-1-2552, N00014-21-1-2909, N00014-13-10291, N00014-15-1-2455, and N00014-18-1-2041). We are also grateful for support from the Division of Mathematical Sciences and the Division of Polar Programs at the US National Science Foundation (NSF) through grants DMS-2309520, DMS-0940249, DMS-2136198, DMS-2111117, DMS-2206171, DMS-1715680, and DMS-1413454. Finally, we would like to thank the NSF Math Climate Research Network (MCRN), and especially Chris Jones, for supporting this work.

## References

- [1] M. Avellaneda and A. Majda. Stieltjes Integral Representation and Effective Diffusivity Bounds for Turbulent Transport. *Phys. Rev. Lett.*, 62:753–755, 1989.
- [2] M. Avellaneda and A. Majda. An Integral Representation and Bounds on the Effective Diffusivity in Passive Advection by Laminar and Turbulent Flows. *Comm. Math. Phys.*, 138:339–391, 1991.
- [3] G. A. Baker and P. R. Graves-Morris. *Padé Approximants*. Encyclopedia of Mathematics and its Applications. Cambridge University Press, 1996.
- [4] R. Bhattacharya. Multiscale Diffusion Processes with Periodic Coefficients and an Application to Solute Transport in Porous Media. *Ann. Appl. Probab.*, 9(4):951–1020, 1999.

- [5] L. Biferale, A. Crisanti, M. Vergassola, and A. Vulpiani. Eddy diffusivities in scalar transport. *Phys. of Fluids*, 7:2725–2734, 1995.
- [6] A. Fannjiang and G. Papanicolaou. Convection Enhanced Diffusion for Periodic Flows. *SIAM J. Appl. Math.*, 54(2):333–408, 1994.
- [7] A. Fannjiang and G. Papanicolaou. Convection-enhanced diffusion for random flows. *J. Stat. Phys.*, 88(5-6):1033–1076, 1997.
- [8] G. B. Folland. *Introduction to Partial Differential Equations*. Princeton University Press, Princeton, NJ, 1995.
- [9] G. B. Folland. *Real Analysis: Modern Techniques and Their Applications*. Wiley–Interscience, New York, NY, 1999.
- [10] P. Gonnet, S. Güttel, and L. N. Trefethen. Robust Padé approximation via SVD. *SIAM Review*, 55(1):101–117, 2013.
- [11] A. Majda and P. R. Kramer. *Simplified Models for Turbulent Diffusion: Theory, Numerical Modelling, and Physical Phenomena*. Physics reports. North-Holland, 1999.
- [12] D. McLaughlin, G. Papanicolaou, and O. Pironneau. Convection of Microstructure and Related Problems. *SIAM J. Appl. Math.*, 45:780–797, 1985.
- [13] R. M. McLaughlin and M. G. Forest. An anelastic, scale-separated model for mixing, with application to atmospheric transport phenomena. *Phys. of Fluids*, 11(4):880–892, 1999.
- [14] R. C. McOwen. *Partial Differential Equations: Methods and Applications*. Prentice Hall PTR, 2003.
- [15] N. B. Murphy, E. Cherkaev, J. Xin, J. Zhu, and K. M. Golden. Spectral analysis and computation of effective diffusivities in space-time periodic incompressible flows. *Ann. Math. Sci. Appl.*, 2(1):3–66, 2017.
- [16] N. B. Murphy, E. Cherkaev, J. Zhu, J. Xin, and K. M. Golden. Spectral analysis and computation for homogenization of advection diffusion processes in steady flows. *Journal of Mathematical Physics*, 61(1):013102, 2020.
- [17] A. Novikov, G. Papanicolaou, and L. Ryzhik. Boundary layers for cellular flows at high Péclet numbers. *Comm. Pure Appl. Math.*, 58(7):867–922, 2005.
- [18] G. A. Pavliotis. *Homogenization theory for advection-diffusion equations with mean flow*. PhD thesis, Rensselaer Polytechnic Institute Troy, New York, 2002.
- [19] G. A. Pavliotis and A. Stuart. *Multiscale Methods: Averaging and Homogenization*. Texts in Applied Mathematics. Springer New York, 2008.
- [20] M. C. Reed and B. Simon. *Functional Analysis*. Academic Press, San Diego CA, 1980.
- [21] H. L. Royden. *Real Analysis*. Prentice-Hall Of India Pvt. Limited, third edition, 1988.
- [22] I. Stakgold. *Boundary Value Problems of Mathematical Physics*. Classics in Applied Mathematics. SIAM, 2000. 2-volume set.
- [23] M. H. Stone. *Linear Transformations in Hilbert Space*. American Mathematical Society, Providence, RI, 1964.
- [24] G. I. Taylor. Eddy motion in the atmosphere. *Philos. Trans. Royal Soc. A*, 215(523–537):1–26, 1915.
- [25] G. I. Taylor. Diffusion by continuous movements. *Proceedings of the London Mathematical Society. Third Series*, 2:196–211, 1921.